12-3-2013

Improvement of Dynamic Performance of the Grid Connected Photovoltaic (PV) System by Series Compensating Devices

Md Kamal Hossain

IMPROVEMENT OF DYNAMIC PERFORMANCE OF GRID CONNECTED

PHOTOVOLTAIC (PV) SYSTEM BY SERIES COMPENSATING DEVICES

by

Md Kamal Hossain

A Thesis

Submitted in Partial Fulfillment of the

Requirements for the Degree of

Master of Science

Major: Electrical and Computer Engineering

The University of Memphis

December 2013

This thesis is dedicated to my parents, my brothers, my uncle, aunty and my cousins for all their love and support they gave me.

ACKNOWLEDGEMENTS

PREFACE

Two papers resulting from my research are used as the manuscript of this thesis. One article was published in the Proceedings of *2013 IEEE SoutheastCon Conference*. The other article has been accepted for presentation at the 2014 IEEE PES Transmission & Distribution Conference & Exposition. Following is a list of the articles used as chapters in this document:

Chapter 3: Md Kamal Hossain and Mohd. Hasan Ali, "Low Voltage Ride Through Capability Enhancement of Grid Connected PV System by SDBR", accepted and will be presented at the 2014 IEEE PES Transmission & Distribution Conference & Exposition.

Chapter 4: Md Kamal Hossain and Mohd. Hasan Ali, "Small Capacity Energy Storage for Power Fluctuation Minimization with Spatially Diverged PV Plant," Proceedings of *2013 IEEE SoutheastCon Conference,* Jacksonville, FL, April 4-7, 2013.

ABSTRACT

Hossain, Md Kamal M.S. The University of Memphis. December 2013. Improvement of dynamic performance of the grid connected Photovoltaic (PV) system by series compensating devices. Major Professor: Dr. Mohd Hasan Ali.

This study proposes the bridge type fault current limiter (BFCL) and series dynamic braking resistor (SDBR) methodologies to enhance the low voltage ride through (LVRT) capability of the PV plant during network faults. This work also focuses on smoothing out the PV power fluctuation due to variable irradiance. To achieve this, the output power of diversely located identical and small PV plants, instead of a big PV plant in a certain area, is integrated. Simulations performed through the Matlab/Simulink software shows that the terminal voltage obtained from the proposed protection schemes maintains the grid code, and hence the PV systems need not to be disconnected from the grid during fault. It is also seen that smoothing of PV power fluctuation is possible by the proposed integration method. Also, the size of the energy storage required for the diversely located PV system is smaller than that for a big PV plant.

TABLE OF CONTENTS

LIST OF TABLES

LIST OF FIGURES

I. INTRODUCTION

A. *Background Study on Photovoltaic (PV) Power*

The world energy demad is increasing rapidly and it will increase up to 53% by 2035 [1]. The increase of usage of renewable energy sources over the past few decades is playing a vital role in solving the acute energy demand problems and environmental concern issue like global warming. As a renewable energy source, photovoltaic (PV) has attracted the attention due to their sustainability, cleanliness, maintenance free and omnipresent behavior. Recently, PV cells, which convert solar energy into the electrical energy, have been widely exploited in applications such as wireless sensor networks (WSNs), autonomous systems, and power plant systems [2]. According to the International Energy Agency (IEA) [3], the PV industry around the world has developed at an average annual growth rates of 15% to 20% from 1991 to 2007, which is comparable to that of the semiconductor and computer industries [4]. It is seen from figure.1 that, in the last 13-year period (from 2000 to 2012), global cumulative installed photovoltaic power has increased from 1,400 MW to 102,156 MW [4] [5].

	2000	2001	2002	2003	2004	2005	2006	2007	2008	2009	2010	2011	2012
Europe	129	262	396	598	1305	2289	3281	5310	11020	16850	30472	52884	70043
APAC	355	495	686	916	1198	1500	1825	2096	2631	3373	4956	7628	12397
America	146	178	225	290	394	501	650	863	1209	1752	2780	4959	8717
China	19	24	42	52	62	70	80	100	140	300	800	3300	8300
MEA	0	0	0	0	1	1	1	2	3	25	71	192	601
ROW	751	807	887	964	993	1003	1108	1150	1226	1306	1590	2098	2098

Figure 1. Worldwide cumulative PV power installed [5].

Table 1 represents some advantages and disadvantages of PV [6].

Table 1. Advantage and disadvantages of Photovoltaic power [6].

Advantages	Disadvantages
There is unlimited stock of fuel (i.e. solar irradiance) .	Fuel source (i.e. solar irradiance) is intermittent in nature.
Environment friendly, since it nether produces waste nor produces noise because of not having any moving part.	
Operation and maintainance cost is minimum.	Initial installation cost is high.
It is capable of operating at normal temperature, hence, no high temperature	
It has long lifetime after installation (>20 years).	It requires expensive energy storage device for proper delevering of the harvested power.
Installation process is very rapid.	External installation devices(e.g. base of system(BOS)) are required for proper facing of the solar cell to the sun.
It can be installed at existing or new residintial buildings.	
It can be installed near to the load.	
Local demand may match with the peak generation.	Efficient energy storage systems can incur large amount of installation cost.
It has high public demand.	
Safety record is excellent.	

B. Photovoltaic System Basic

a. Working Principle of a Solar Cell

A PV cell as shown in figure 3 is basically a semiconductor diode whose p–n junction is exposed to light [7]. When the sunlight impinges on the PV cell, electron-hole pairs are created by the interaction of the incident photons and the atoms of the PV cell. However, all the photons are not capable of producing the electron-hole pair. Those photons that have the energy greater than the bandgap energy of the semiconductor material are only capable of generating the electron-hole pairs. The built in potential or electric field at the

3

p-n junction of the PV cell causes the photon- generated-electron-hole pairs to separate, with electron drifting into the n-region (e.g. phosphorus-doped) and hole drifting in the p-region (e.g. boron-doped) as shown in figure 2. A specially made selective contact is employed to collect the electrons from the n-region and these electrons are conveyed to the external circuit. The electrons release their energy by doing work in the external circuit such as pumping water, spinning a fan, powering a sewing machine motor, a light bulb, or a computer [6].
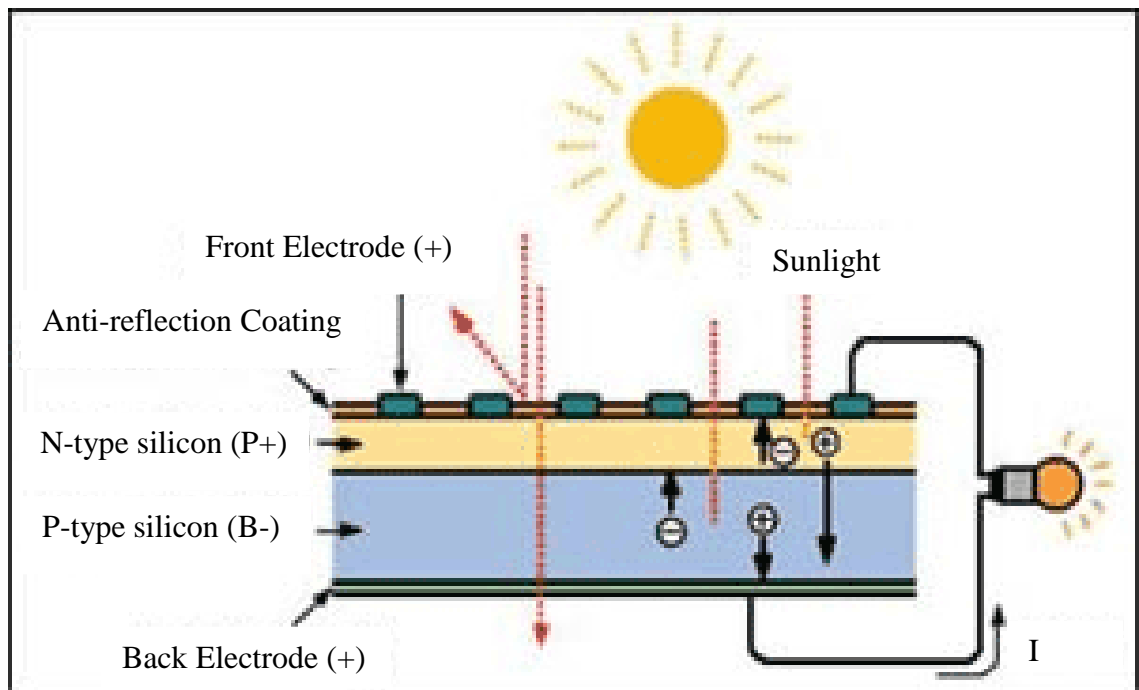
Figure 2. Construction of solar cell [8].

Figure 3. Picture of a solar cell [9].

Typical voltage difference of a solar cell is 0.5V as long as the cell is illuminated with sunlight [9]. The field of solar cell fabrication and characterization is an interesting area of research and it is beyond the scope of this thesis.

b. *PV module and array modeling*

PV power is generated to employ numerous applications ranging from small scale (e.g. wireless sensor network) to large scale (e.g. grid supply). PV cells are connected in series to form PV module and the PV module is encapsulated in an environmentally protected element. PV modules are connected in series-parallel combination to obtain higher voltages or currents [10]. If the requirement is higher voltage, then the series connection of the PV modules is employed whereas for the higher current parallel connection is employed. Figure 4 illustrates the elements of the PV system.
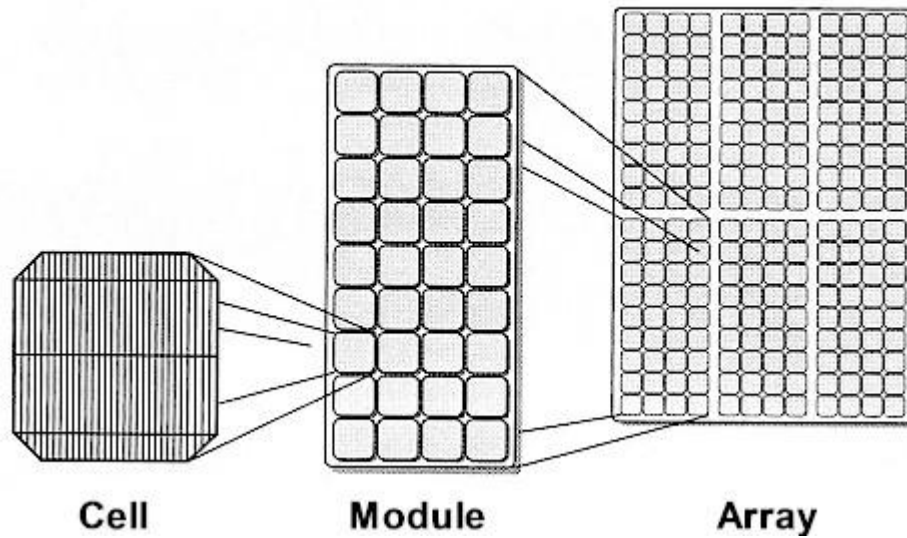
Figure 4. PV cell, module and array [11].

Figure 5 represents the characteristic curve (I-V curve) of a PV module. The I–V curve in Figure 5 shows three very important points: short circuit (0, I_{SC}), MPP (V_{mp} , I_{mp}), and open circuit (V_{OC} , 0). The PV cell has both limiting voltage and limiting current and hence the cell is not damaged by operating it under either short-circuit or open-circuit conditions [10]. A particular PV module is capable of delivering the maximum voltage (V_{mp}) and current (I_{mp}) at particular environmental condition (irradiance and temperature).
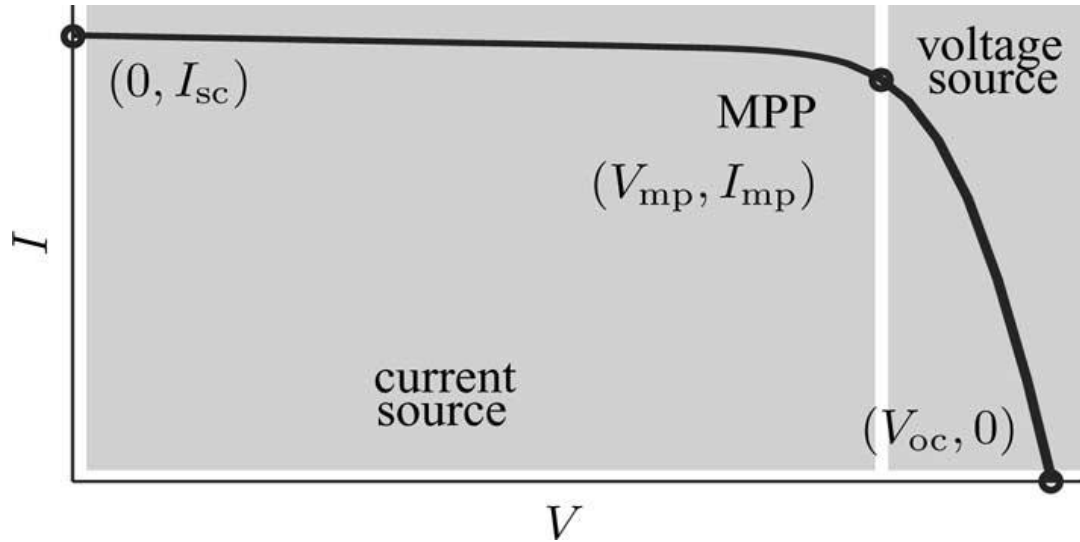
Figure 5. I–V Characteristic curve of a practical PV module [7].

Figure 6 represents that the higher voltage is attained by connecting m number of PV modules in series whereas the higher current is obtained by parallel connection of n number of PV modules which is shown in figure7. A large PV array consists of a large number of PV modules as shown in figure 8. m identical modules form of a PV string and n identical PV strings are connected in parallel to build a large PV array. The open-circuit voltage and the short-circuit current are ($m \times V_{OC}$) and ($n \times I_{SC}$) respectively.
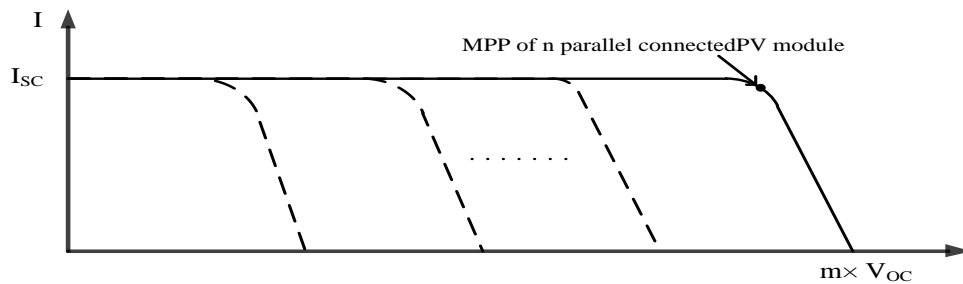
Figure 6. I–V Characteristic curve of a PV string with 'm' modules in series [4]
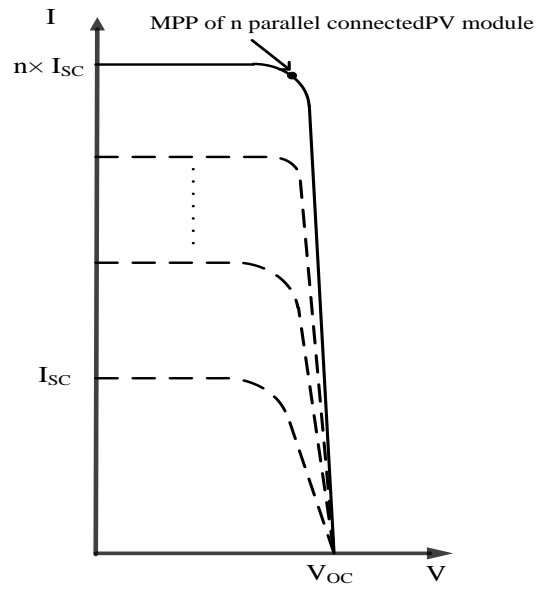
Figure 7. I–V Characteristic curve of a PV string with 'n' modules in parallel [4].
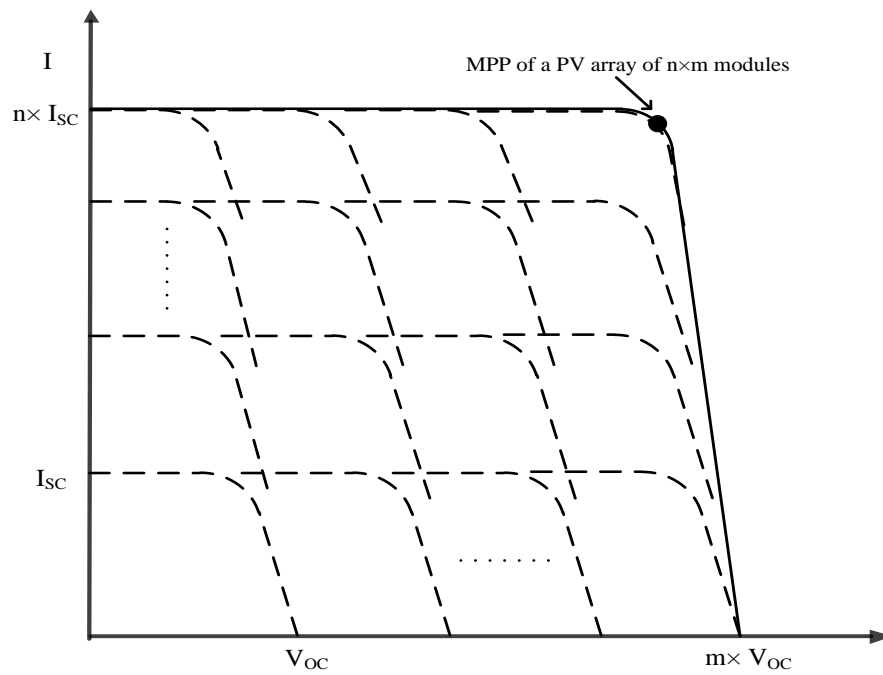
Figure 8. I–V Characteristic curve of a PV array of 'm×n' modules connected in series-parallel configuration [4].

c. Bypass and blocking diodes

When a PV array is exposed to the partial shading condition, hot-spots may appear at the less illuminated modules. Bypass diodes are connected to the PV modules to avoid hot-spot condition. In practice, it is sufficient to connect one bypass diode for every 15-20 cells [12]. The blocking diode is connected in series with each string, which is a group of series-connected PV modules, to protect the modules from the effect of the potential difference between series-connected strings [13] as shown in figure 9 (a). Although only one MPP is exhibited on the *P–V* characteristic curve in the presence of uniform insolation, multiple local MPPs can be exhibited because of the bypass and blocking diodes when partial shading condition (PCS) appears as shown in figure 9(c).
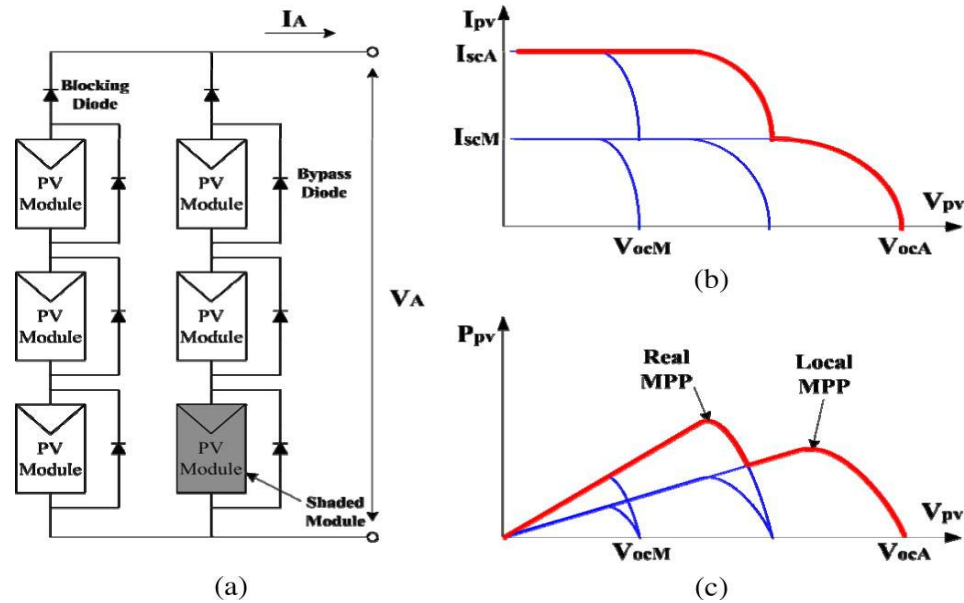
Figure 9. Characteristics of a PV array under partially shaded conditions. (a) PV array configuration. (b) I–V characteristics. (c) P –V characteristics [13].

II. PV MODELING AND SIMULATION

PV modeling is related to the determination of the characteristic curves (P-V and I-V curve) under different weather conditions to follow the real solar cell [14]. There are different types of PV modeling available in the literature; the simplest one is the basic single diode model. The equivalent electrical circuitry of a PV cell is shown in Figure 10, in which the simplest single diode is represented by a constant current source in antiparallel with a diode, and the non-idealities are represented by the insertion of the resistances *Rs* (series resistance) and *R$_P$* (parallel resistance) [15]. The model requires five parameters to completely characterize the I–V curve, namely short-circuit current (I$_{sc}$), open circuit voltage (V$_{oc}$), diode ideality factor (a), series resistance (Rs) and parallel resistance (R$_P$) [14]. In the single diode model, recombination loss in the depletion region is neglected; however, the presence of this particular loss is substantial in practical case [16]. Considering this loss, a more accurate two diode model is proposed in [16] [17]. Introducing second diode in the PV model incurs the burden of determining another parameter. The equivalent circuit of two diode model is shown in figure11. The accurate modeling of the PV cell is a vast area of research and it is beyond the scope of this particular thesis.
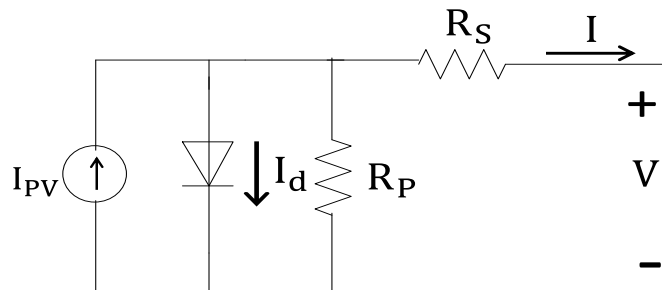
Figure 10. Single diode model of a PV cell [16].

10
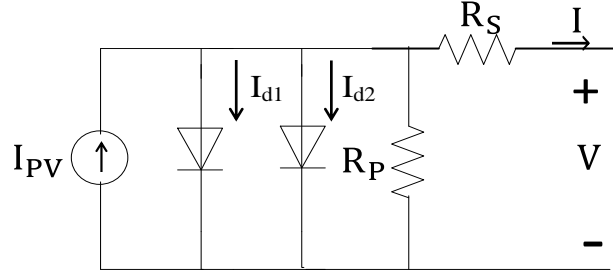
Figure 11. Two diode model of a PV cell [16].

The single diode model shown in figure 10 is employed to simulate the PV cell in this thesis and equation (1) is the solar cell current equation for this model.

$$I = I_{PV,cell} - I_{0,cell}\left[e\left(\frac{V + R_S I}{V_t a}\right) - 1\right] - \frac{V + R_S I}{R_P} \tag{1}$$

where V and I represent the PV cell output voltage and current, respectively. $V_t = kT/q$ is the thermal voltage of the diode, R_S and R_P are the equivalent series and shunt resistances of the cell, respectively. q is the electron charge ($1.6 \times 10-19$ C); $I_{PV,cell}$ is the light generated current, $I_{0,cell}$ is the reverse saturation current, a is the ideality factor of the diode, k is Boltzmann constant 1.38×10^{-23} JK^{-1}, and T is the temperature (in Kelvin).

A. *Modeling of a PV module*

Since PV arrays are composed of large numbers of solar cells, it is impractical to simulate all the cells individually in a PV array. Manufacturer of the solar panel provides modules rather than the solar cell and these solar cells sustain the same characteristic. Therefore, the solar module can be considered as the building block for the large PV array. The basic equation represented by the equation (1) requires some modifications to represent it as the solar module equation [7].

11

$$I = I_{PV} - I_0 \left[e\left(\frac{V + R_S I}{V_t a} \right) - 1 \right] - \frac{V + R_S I}{R_P} \tag{2}$$

where V_{PV} and I_{PV} represent the PV module output voltage and current, respectively. $V_t = N_s kT/q$ is the thermal voltage of the module with N_s cells connected in series, R_S and R_P are the equivalent series and shunt resistances of the module, respectively. The light-generated current I_{PV} depends on the irradiance and temperature, which can be represented by the following equation [7]:

$$I_{PV} = (I_{PV,n} + K_I \Delta T) \frac{G}{G_n} \tag{3}$$

where $I_{PV,n}$ is the light-generated current of the module at nominal temperature and irradiation (usually 25^0 C and 1000 W/m^{-2}), ΔT is the difference between actual and nominal temperature, K_I is the short-circuit current temperature coefficient, G and G_n are actual and nominal irradiation, respectively. In this thesis, the equation employed for saturation current I_0 [7] is:

$$I_0 = \frac{I_{SC,n} + K_I \Delta T}{e(q(V_{OC,n} + K_V \Delta T)/V_t a) - 1} \tag{4}$$

where $I_{SC,n}$ and $V_{OC,n}$ are the short circuit current and open circuit voltage of the module at nominal condition, respectively, and K_V is the open circuit voltage temperature coefficient.

B. *Matlab Simulation of PV module*

The mathematical model of the PV module is implemented in the MATLAB/Simulink Software. The reason for choosing the MATLAB/Simulink simulation environment is that it has an excellent SimPowerSystems toolbox, which has a great facility to interface the modeled PV system with the conventional power, electrical and control systems.

This thesis implements the equivalent circuit model shown in figure 10. Although two simulation methods are mentioned in [7], a circuit model exploiting one current source (I_m) with two resistors is used which is shown in figure 12.
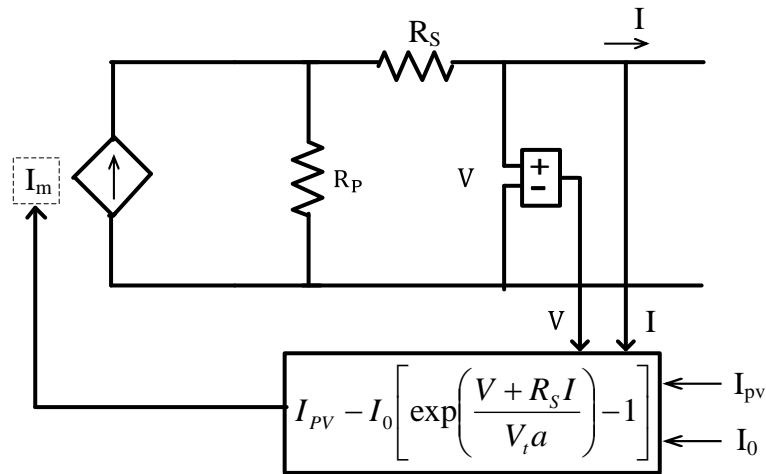
Figure 12. Modeling circuit of PV module [7].

The circuit described in figure 13 is implemented in MATLAB/Simulink. It is seen from the above model that V, I, I_{pv} and I_0 are employed to compute the model current I_m. I_{pv} and I_0 are calculated from the equations (3) and (4) respectively.

Although some parameters are provided by the manufacturer of the solar cell, however, two parameters such as R_s and R_p are still unknown. These two parameters are

13

very important parameter to design a solar module correctly. Authors in [7] employed an iterative technique to determine the values of R_s and R_p. In this thesis, the KC200GT PV module [18] data specifications are employed to design the PV model. Table 2 represents the data of KC200GT PV module at standard weather condition (25^0C, AM 1.5 and 1000 w/m^2). The values of R_s and R_p are 0.221 ohm and 415.405 ohm, respectively, and they are taken from [7].

Table 2. Parameters of the KC200GT Solar module at 250C, AM 1.5, 1000 w/m2 [7]

Peak Power (P_{max})	200 W
Voltage at maximum power V_{max}	26.3 V
Current at maximum power I_{max}	7.61A
Number of solar cells per Module N_S	54
Open Circuit Voltage (V_{OC})	32.9
Short Circuit Current (I_{SC})	8.21A
Temperature Coefficient of $I_{SC,}$ K_I	0.0032 A/K
Temperature Coefficient of $V_{OC,}$ K_V	-0.1230 V/K
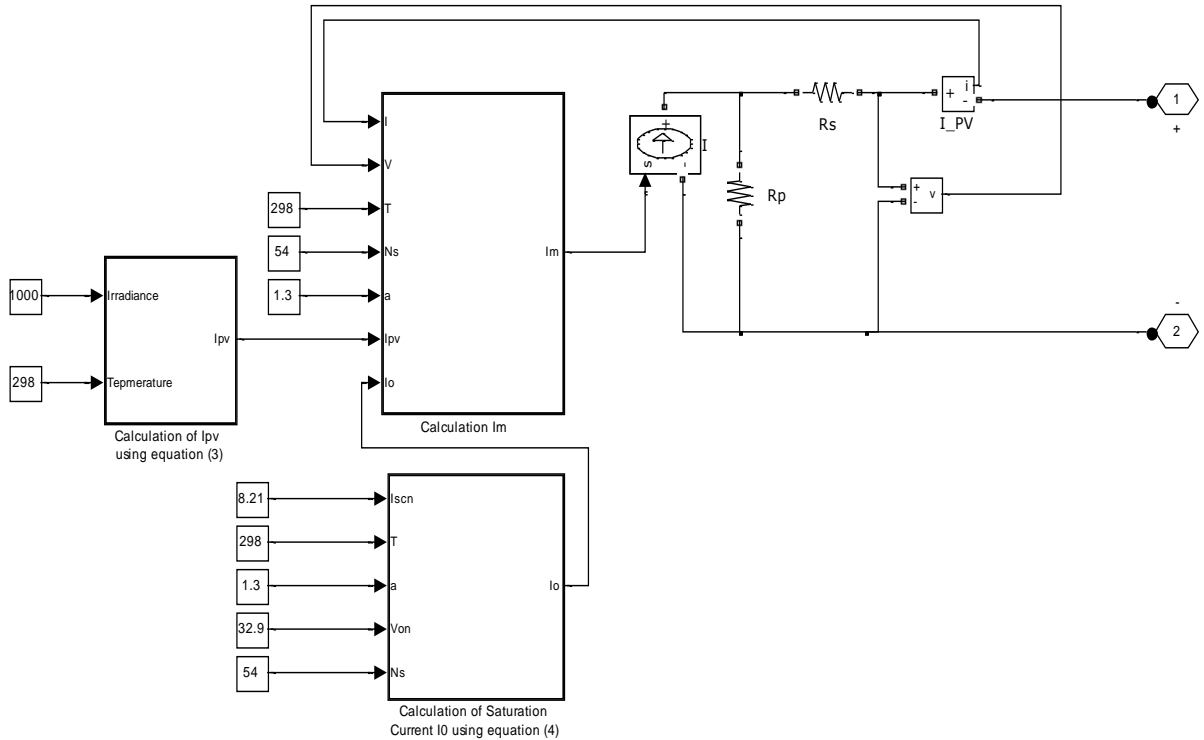
Figure 13. MATLAB/Simulink model for PV module.

From the above simulation model, it is seen that the I_m is computed from I_{pv}, I_0, the feedback voltage (V) and current (I). The PV characteristics curves for this model are presented in figures 14, 15, 16, and 17. It is evident from the I-V curves represented in figure 14 that the magnitude of the PV module current is mostly affected by the irradiance change; however, the change of voltage is not that much noticeable with the irradiance change. The change of temperature causes the noticeable change of the voltage, i.e., voltage decreases incrementally with the temperature; however, the change of current is not prominent with the change of temperature [7]. The change of PV power with constant temperature and variable irradiance is presented in figure15. Figure 17 represents the change of PV power with variable temperature and constant irradiance.
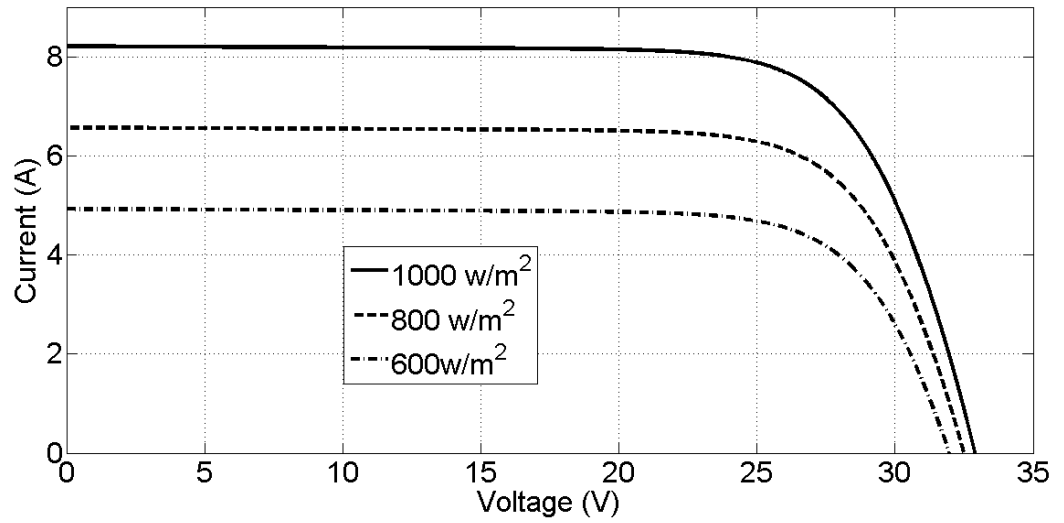
Figure 14. I-V curves of the KC200GT PV module at 250 C temperature and different irradiance conditions.
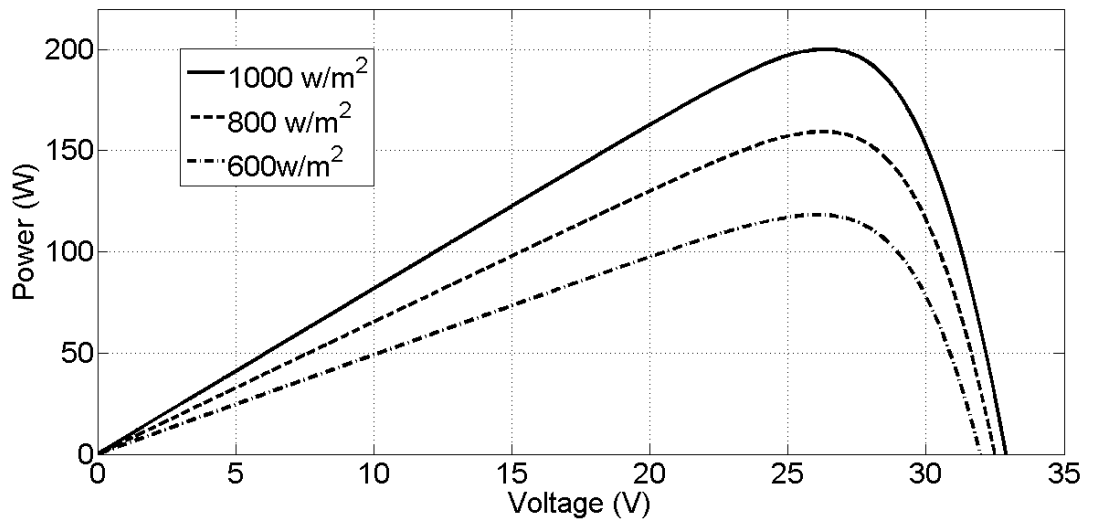
Figure 15. P-V curves of the KC200GT PV module at 250 C temperature and different irradiance conditions.
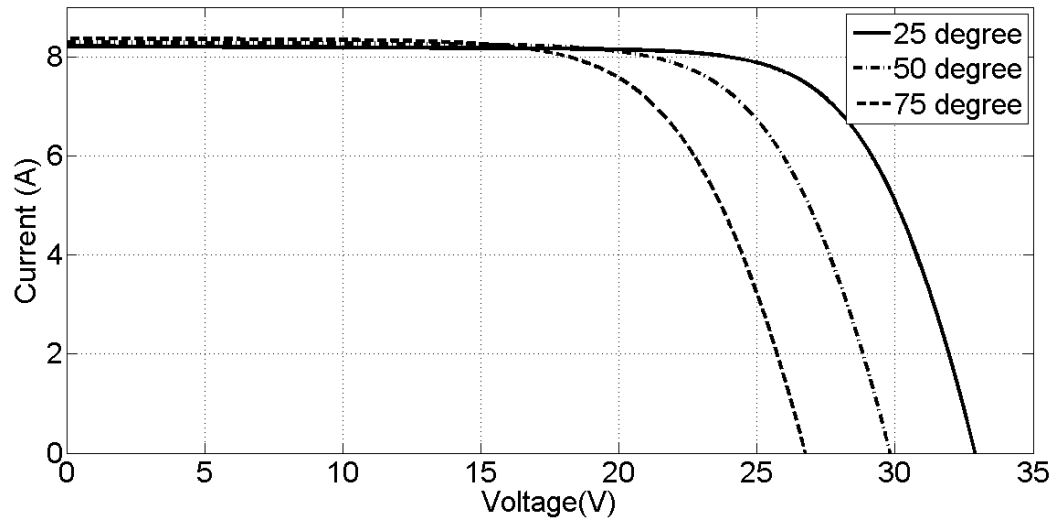
Figure 16. I-V curves of the KC200GT PV module at 1000 w/m2 irradiance and different temperature conditions.
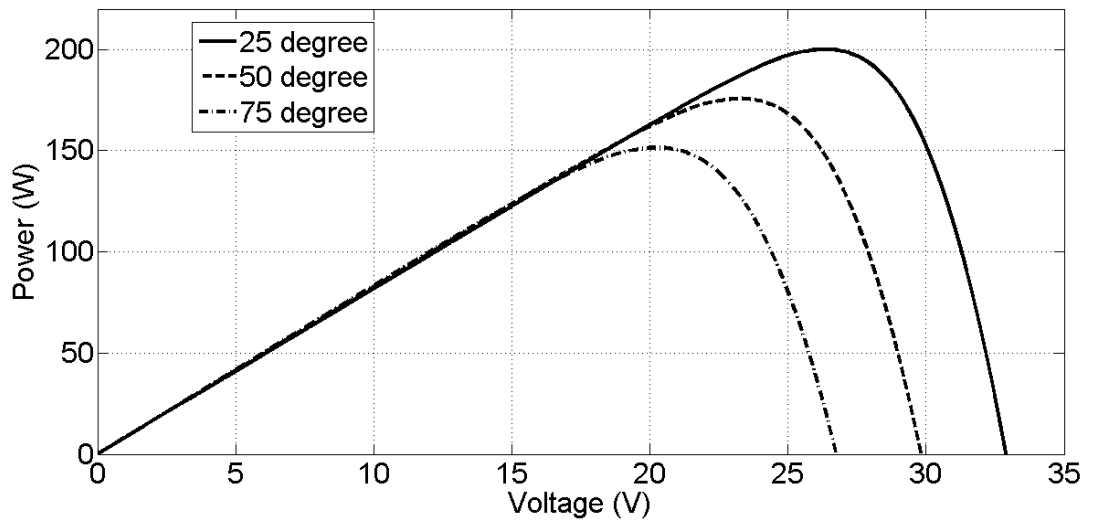
Figure 17. P-V curves of the KC200GT PV module at 1000 w/m2 irradiance and different temperature conditions.

C. *Large PV arrays*

A large PV array is composed of several PV modules connected in series-parallel combination to obtain large-scale power. PV array can be designed by inserting the

equivalent open-circuit voltage and short-circuit current in the previously designed model of PV module. This section is devoted to explain the procedure of modeling of the large PV array from the PV modules. In order to simulate the PV array, which is composed of several identical PV modules, the following circuit [19] was implemented in this thesis.
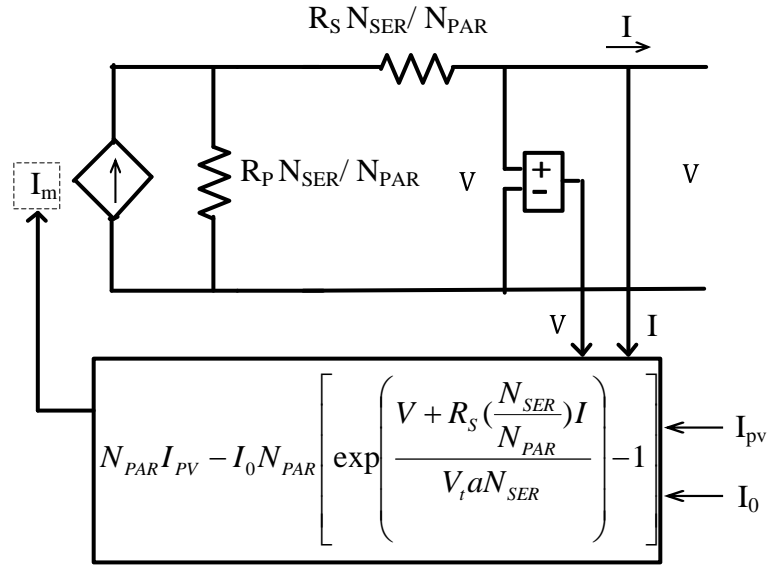
Figure 18. Circuit model of a NPAR× NSER PV array [19].

For a PV array which is composed of $N_{PAR} \times N_{SER}$ PV modules, the following equation is applicable [19].

$$I = N_{PAR}I_{PV} - I_0 N_{PAR}\left[\exp\left(\frac{V + R_S(\frac{N_{SER}}{N_{PAR}})I}{V_t a N_{SER}}\right) - 1\right] - \frac{V + R_S(\frac{N_{SER}}{N_{PAR}})I}{R_P R_S(\frac{N_{SER}}{N_{PAR}})} \tag{5}$$

where I_{PV}, I_0, R_S, R_P, and V_t are parameters of individual modules. Figure 20 represents the I-V and P-V characteristics of the designed PV array and it is evident from the figure19 that it has 0.5MW peak power rating. In this manner, a large PV plant can be modeled. Table 3 represents the parameters of the 0.5 MW PV array model.
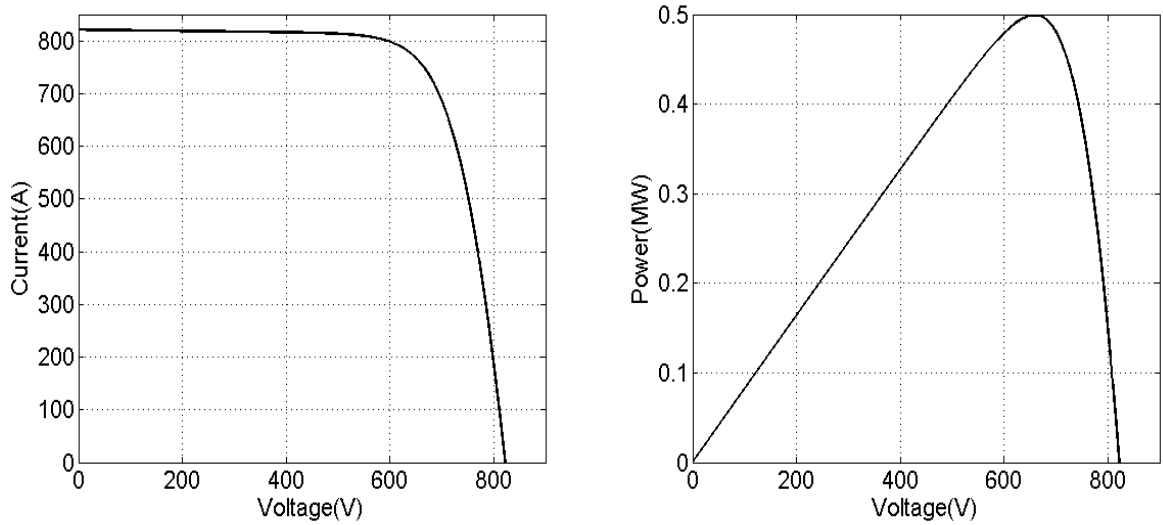
Figure 19. I-V and P-V characteristics of the PV 0.5MW PV array.

Table 3. Parameters of 0.5MW PV plant, which is composed of KC200GT solar module.

Peak Power (P_{max})	0.5MW
Voltage at maximum power V_{max}	658.85V
N_S	54
N_{ser}	25
N_{par}	100
R_S	0.05525Ω
R_P	103.85Ω

D. Modeling of Grid-Connected PV System

Normally, a grid connected PV system consists of a PV array, a maximum power point

tracking technique (MPPT) technique which is employed to extract the maximum power

from the PV array, an inverter to integrate the PV power to the grid. All the protection

schemes required to protect the PV array is mounted there. The MPPT techniques are

sometime employed on dc-dc converter or to the inverter.

Figure 20 represents the schematic diagram of the grid connected 0.5 MW (peak) PV

plant. The PV plant is connected through the DC/DC boost converter and then a DC/AC

inverter is employed to dispatch the AC power to the grid. The inverter is capable of

maintaining constant 1kV DC voltage at the DC link. Finally a 0.420 kV/ 11kV

transformer (delta-way) is employed to integrate the generated PV power to the grid.

Figure 21 represents the responses of the PV power, voltage measured at the immediate

PV terminal, and duty cycle applied to the boost converter with variable irradiance

profile. It is seen from figure21 that when the irradiance level is 1000 w/m^2, the PV plant

is delivering 0.5 MW power to the grid. However, when the irradiance level goes down to

250 w/m^2, it is delivering about 0.115 MW power. The duty cycle is varied by the MPPT

technique to extract the maximum power at different irradiance levels.
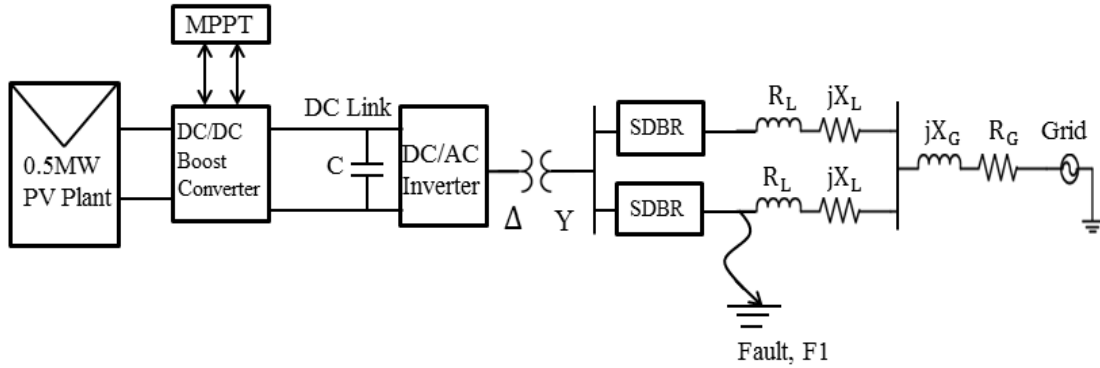
Figure 20. Schematic of grid connected system.
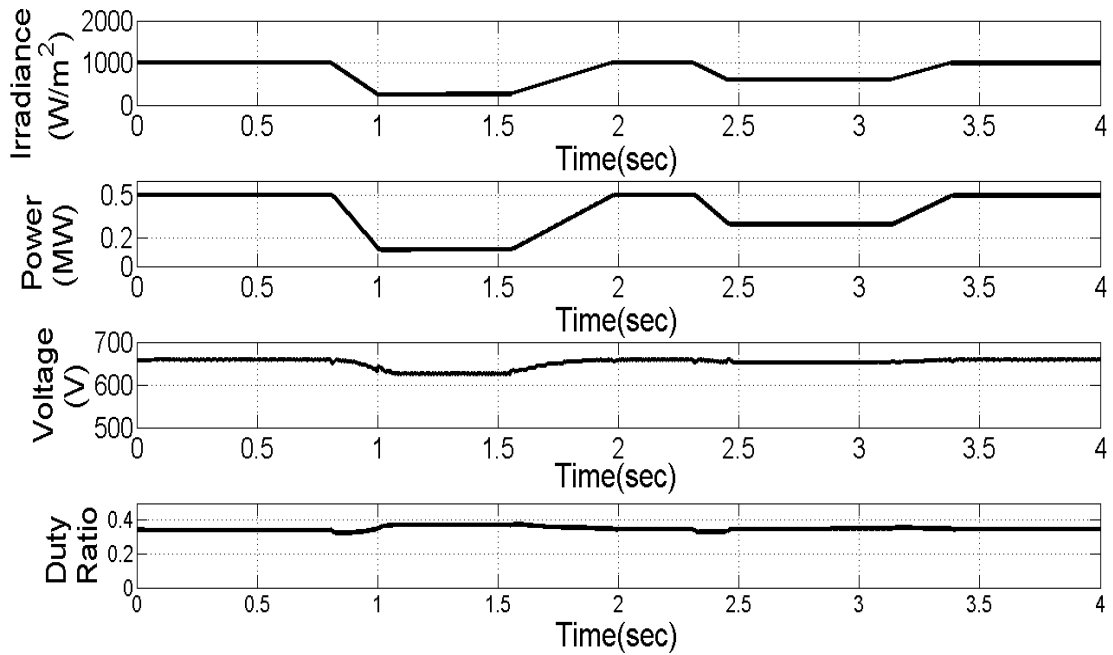
Figure 21. Responses of the 0.5 MW peak PV plant with variable irradiance.

a) Maximum Power Point Tracker (MPPT)

PV system depicts nonlinear P-V characteristics and it has only one maximum

operation point or maximum power point (MPP) for a particular environmental condition.

The PV arrays operating other than this particular MPP might be accompanied with

substantial and sustained power loss. In order to maximize the overall efficiency of the

PV generator, an MPPT technique which is capable of extracting the maximum power from the PV generator needs to implement with PV energy harvester.

A large number of MPPT techniques are available in the literature [20]. Different MPPT techniques have different features considering cost, complexity, sensor required and tracking speed, and it is very confusing which techniques are suitable for particular applications. In this thesis, the MPPT technique is employed to the DC/DC boost converter. The PV system and the DC link are connected to the input and output of the boost converter, respectively. Some most common MPPT techniques are described below:

b) Perturb and Observe (P&O) Method

Different techniques are employed to address the issue of MPPT techniques, however, for low cost and ease of commercial implementation, the perturb and observe (P&O) MPPT algorithm is commonly exploited [21]. This is a simple method and it does not require previous knowledge of the PV generator characteristics or the measurement of solar intensity and cell temperature and also easy to implement with analogue and digital circuits [22]. The P&O algorithm perturbs (increasing or decreasing the control parameter by a small amount) the operating point in a particular direction and measures the power. The measured power after the perturbation is compared with the power before the perturbation. As shown in figure 22, if the power increases, i.e. change of power in the same direction (dP/dV>0), then the algorithm also maintains the perturbation in the same direction. However, if the change of power in opposite direction (dP/dV<0), the algorithm perturbs the system in the opposite direction. A P&O based controller causes the PV voltage take the sequence of values V(k) [23] as follows:

$$V(k+1) = V(k) + \Delta(k-1); P_k \geq P_{k-1} \qquad (6)$$

$$V(k+1) = V(k) - \Delta(k-1); P_k < P_{k-1} \qquad (7)$$

Where, Δ is the P&O step size, and V(k) and P(k) denote the panel output voltage and measured power sequences, respectively.
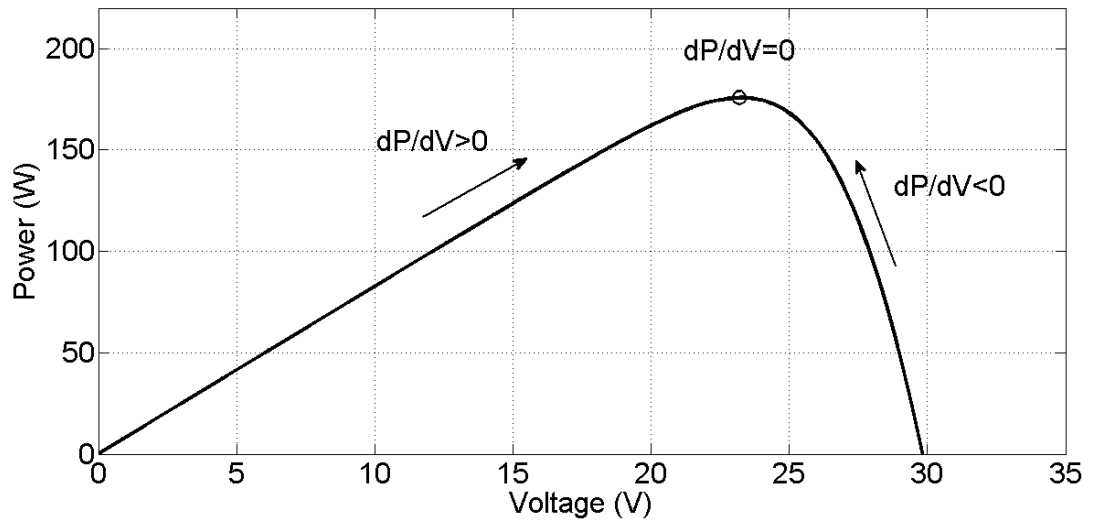
Figure 22. Perturb and Observe (P&O) Method.

c) *Fractional Open-Circuit Voltage (FOCV) Method*

In fractional open-circuit voltage method [24], the cell voltage (V_m) corresponding to the maximum power exhibits a linear relationship with cell open circuit voltage (V_{oc}) as follows:

$$V_m \approx k_1 V_{oc} \qquad (8)$$

The above relationship is independent of panel configuration, and the constant k_1 is called the voltage factor which is equal to 0.71 for the silicon panel [24]. Despite of being a simple method, momentarily opening the load from the PV panel to measure V_{oc} incurs the power loss. In [25], an unloaded pilot PV panel, with characteristics similar to those of the main PV panel and installed under similar conditions, is used to measure the open circuit voltage.

d) Fractional Short-Circuit Current-Based Method

This method is based on the fact that the MPP operating current, I_m is proportional to the short-circuit current, I_{sc} under various irradiance conditions as follows [26].

$$I_m \approx k_2 I_{sc} \qquad (9)$$

Where k_2 is the proportionality constant and equation (15) represents that I_m can be determined instantaneously by detecting I_{sc} and that the MPPT can be achieved by giving a current command to a current-controlled power converter [26].

e) Fuzzy logic controlled (FLC) based MPPT

Fuzzy logic controller is a simple nonlinear controller. This controller does not require mathematical modeling of the plant to be controlled. Since the PV is a highly nonlinear system, FLC is used for tracking the MPP for many PV applications [27]. The design of a fuzzy logic controller requires four basic operations: I) fuzzification II) rule base, III) inference engine and IV) defuzzification procedure. During fuzzification, appropriate

membership functions are found out to describe crisp data as shown in figure 23. Four

fuzzy levels such as PB (positive big), PS (positive small), NS (negative small) and NB

(negative big) are used in this case. x and y are the range of values of numerical variable

in the figure 23. All the inputs and outputs of the FLC require this type of membership

function.
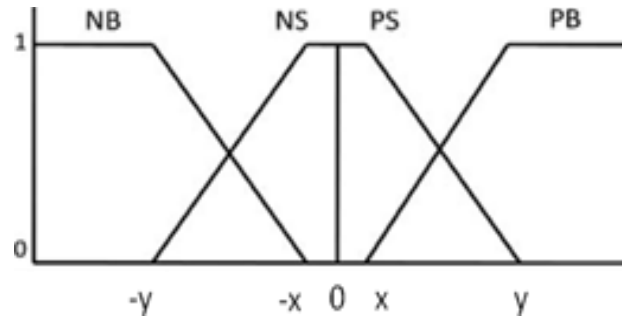
Figure 23. Membership functions [28].

Table 4: Fuzzy Rule Table [27].

CE E	NB	NS	ZO	PS	PB
NB	ZO	ZO	NB	NB	NB
NS	ZO	ZO	NS	NS	NS
ZO	NS	ZO	ZO	ZO	PS
PS	PS	PS	PS	ZO	ZO
PB	PB	PB	PB	ZO	ZO

25

Most of the cases two inputs and one output are used in FLC. Two inputs considered in [27] are

$$E(k) = \frac{P(k) - P(k-1)}{I(k) - I(k-1)} \qquad (10)$$

$$CE(k) = E(k) - E(k-1) \qquad (11)$$

Fuzzy rule based table as shown in table II is needed to be formed where all the entries are fuzzy sets of error $E(k)$, change of error $CE(k)$, and change of duty ratio dD to the boost converter [27]. dD is different for different combination of E(k) and CE(k) and is defined depending on the converter used and the experience of the operator. The defuzzification stage of FLC deals with transformation of linguistic variable to the realistic value to drive the power converter. Therefore, it is seen that the FLC has been exploited extensively for MPP tracking.

f) Incremental Conductance (INC) Method

Among all the MPPT strategies, the incremental conductance (INC) algorithm is widely used due to the high tracking accuracy at steady state and good adaptability to the rapidly changing atmospheric conditions [28]. For this thesis, the incremental conductance (INC) with a simple PI controller [29] is employed as MPPT technique. The basic idea of incremental conductance method is that, the slope of the PV array power versus voltage curve is zero at the MPP [28], positive on the left of the MPP, and negative on the right. This can be rewritten as

26

$dP/dV = 0$, at MPP   (12)

$dP/dV > 0$, to the left of the MPP   (13)

$dP/dV < 0$, to the right of the MPP   (14)

The above relations can be further written in terms of PV system voltage and current by

$$dP/dV = d(IV)/dV = I + V\, dI/dV$$ (15)

According to (3), (4) and (5), the solution of (6) can be written as

$\Delta I/\Delta V = -I/V$ at MPP   (16)

$\Delta I/\Delta V > -I/V$, to the left of the MPP   (17)

$\Delta I/\Delta V < -I/V$ to the right of the MPP   (18)

Therefore, the MPP can be tracked by comparing incremental ($\Delta I/\Delta V$) conductance with instantaneous conductance (I/V). The flowchart of the INC MPPT is depicted in figure 24.
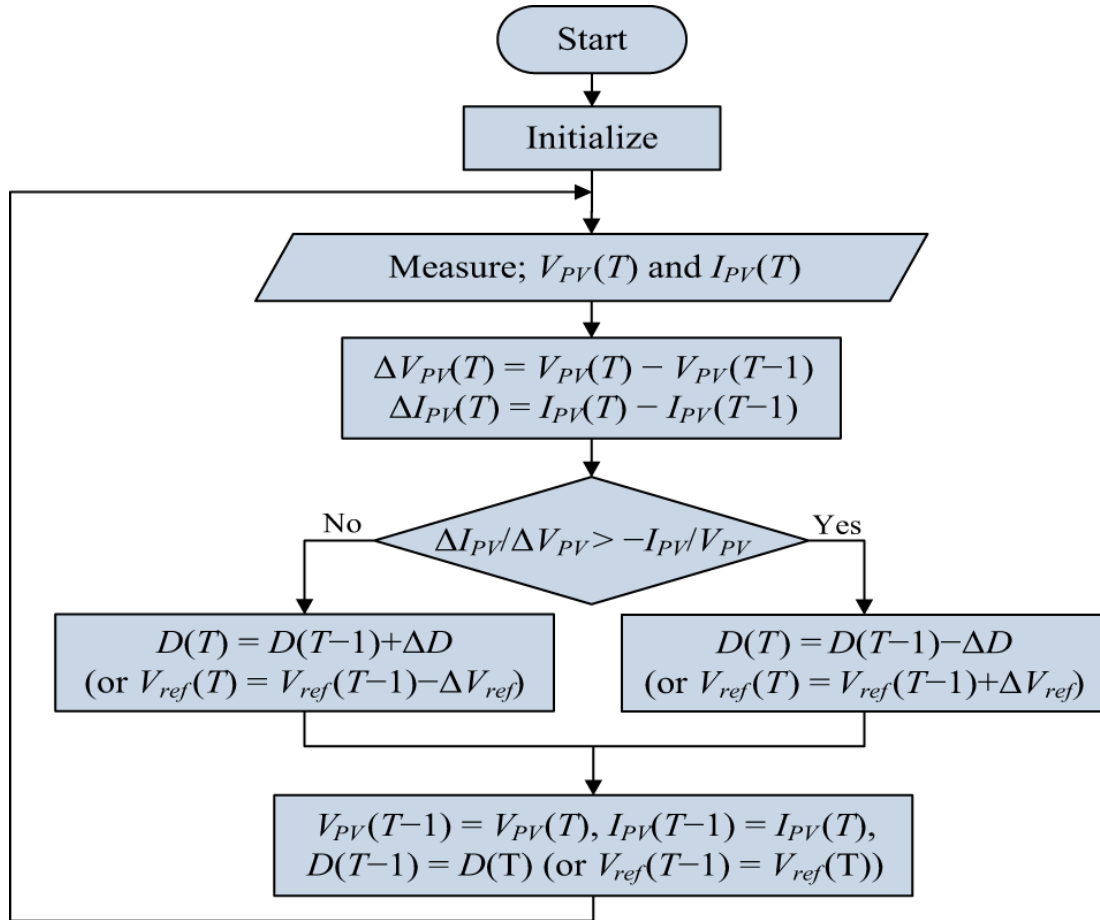
Figure 24. Flowchart of INC method [30].

A simple PI controller minimizes the error between the actual conductance (I/V) and the incremental conductance (ΔI/ΔV). The implementation of the INC method with a PI controller can be represented by Figure 25. The duty cycle generated by this method is employed as the signal to drive the gate of the DC/DC boost converter.
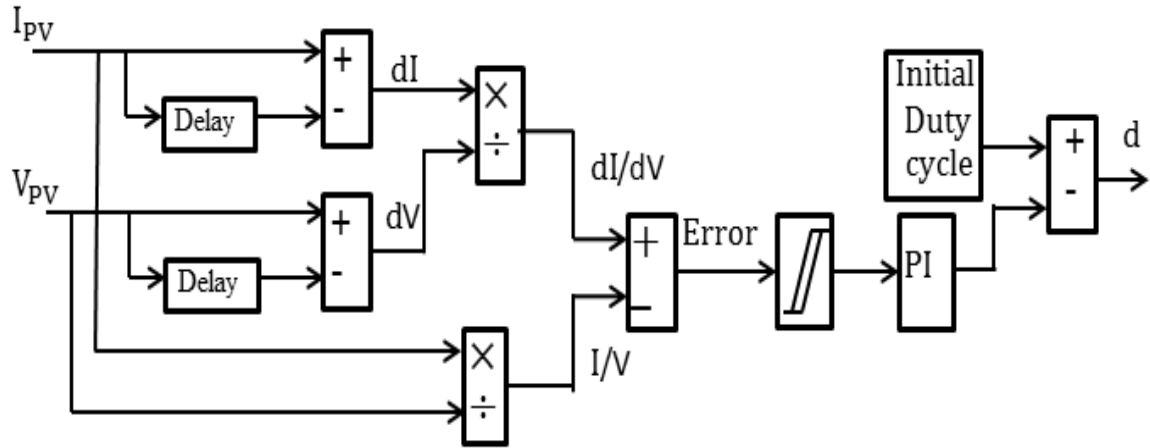
Figure 25. MPPT controller (INC with PI) [29].

E. *Controlling of Voltage Source Inverter (VSI)*

In this work, a widely used vector control technique is employed for the VSI control. The voltage source converter maintains a constant DC link voltage and a power factor of unity. The control mechanism of the VSI is conducted by two control loops, such as an external control loops which regulates the DC link voltage and an internal control loop which regulates the active (I_d) and reactive (I_q) grid current components. The external controller generates the I_d reference current, and I_q current is set to zero for maintaining the unity power factor. Voltage outputs, V_d and V_q, of the internal controller are converted to the three modulating signals which are employed by the PWM pulse generator [31].

III. FAULT RIDE THROUGH CAPABILITY ENHANCEMENT OF GRID CONNECTED PV SYSTEM

Apart from stand-alone PV systems, grid connected megawatt class PV plants are being installed. Present statistics say that over 150 PV parks exist with 10MW or more capacity [32]. Due to high penetration of PV energy in recent times, German grid codes has recently adopted low voltage ride through (LVRT) requirement for PV plants connected to the high [33] and medium [34] voltage power network to maintain dynamic grid support [32].

The operation of power electronic interfaces during extreme voltage disturbance is harmful and can damage power electronic converters [35]. Since grid-connected PV systems are integrated to the grid by power electronic devices, it is extremely important to take remedial steps to prevent the grid disturbance due to fault or any other reasons. One of the most common power frequency disturbances is voltage sag and it is defined as a momentary decrease in the rms voltage, with a duration ranging from half a cycle up to one minute [35].

Previously, the common practice was to disconnect the distributed generators (DGs) (e.g. PV, wind, fuel cell etc.) under voltage sag. As the penetration level of power by DGs is gradually becoming high, disconnection of these DGs from the grid causes power unbalance which may result in power system instability. This means that PV plants must stay connected during a fault, since shutdown of a megawatt class PV plant may have adverse effect in power system operation [32].

In [36] [37], the low voltage ride through (LVRT) characteristics analysis for the penetration of PV power to the grid is reported, but the proposed methods have some shortcomings. Although fault clearing time and location of the faults are focused in [36]

30

and a current source inverter is emphasized in [37] for grid interfacing, however, both works did not consider the MPPT operations during the fault and also the capacity of the PV systems was low. Superconducting fault current limiter (SFCL) is proposed in [35] to prevent voltage sag due to fault on the grid side. Since SFCL is very expensive, it is not a suitable option to use with PV systems. Authors in [32] made an effort to protect the inverter DC link, but this method is not capable of improving the voltage profile of the grid side. Also, it employs fractional open circuit voltage (FOCV) as MPPT technique for big power plant which is impractical, since FOCV requires momentarily opening of the PV terminal. Moreover, all the above mentioned works are considered under constant irradiance which is not feasible, since irradiance is varying all the time.

In this thesis, in order to protect the power electronic devices during voltage sag and increase the low voltage ride through (LVRT) capability of grid connected PV system, two methodologies are proposed, namely I) bridge type fault current limiter (BFCL) [38] and II) series dynamic braking resistor (SDBR) [39]. To the best of my knowledge, both BFCL and SDBR have not been applied before to maintain LVRT capability of the PV systems. Both of these devices are series devices and they come into action before the circuit breaker's opening. They not only reduce the fault current during the grid fault, but also prevent the voltage sag at the PCC by inserting impedance to the fault point. Also, they are simple in construction since they consist of only resistor, inductor and the power electronic switches.

A point to note here is that, in this work we considered variable irradiance. Due to variable irradiance, there will be varying current, which results in varying power; however, the constant voltage is maintained by the controller.

In this chapter, simulation model of grid-connected PV system in chapter 2 is employed to analyze the LVRT capability of the grid connected PV system.

A. PV protection Scheme Under Fault

Table 5 summarizes the protection scheme recommended by the IEEE standard 929 for a grid connected PV system [40] [41]. It indicates that, the protection device disconnects the PV from the grid when it detects grid abnormal voltage or frequency. As the table shows, the time it will take for the protection scheme to disconnect the PV depends on how low the terminal voltage will be during a fault [40]. If the terminal voltage gets below 0.5 pu during the fault, then the PV will be disconnected in less than six cycles or 0.1 sec, however, it may take up to 120 cycles or 2 sec if the terminal voltage remains higher than 0.5 pu [40].

Figure 26 shows the limiting curve of type 2 plants (such as PV) [32], [42]. A plant must not disconnect during the voltage drop down 0% of the nominal voltage (U_c) with a duration of less than or equal to 150ms and should recover the 90% of the voltage from its pre-fault level within 1500ms from the occurrence of the voltage dip [32], [42]. Voltage dips with values above borderline 1 in figure26 may not lead to disconnection or instability [42]. Voltage dips above borderline 2 and below borderline 1 in figure 26 should also be ridden through [42]. According to our proposed method, during fault period, the control devices will limit the fault current and hence raise the voltage. Therefore, the PV plant will be connected to the grid all the time.

Table 5: Protection Scheme for a PV System [40] [41].

		trip time
Terminal voltage	V < 0.5pu	6 cycles
	0.5pu ≤ V < 0.88pu	120 cycles
	0.88pu ≤ V < 1.1pu	normal operation
	1.1pu ≤ V < 1.37pu	120 cycles
	1.37pu ≤ V	2 cycles
grid freq.	f < 59.3	6 cycles
	59.3 ≤ f ≤ 60.5	normal operation
	60.5 < f	6 cycles

Figure 27 shows the location of the fault and the breaker with the proposed BFCL and SDBR. Since the SDBR and BFCL are the series devices, they will come into the action immediately after the fault initiation. When the SDBR or BFCL is installed, they not only reduce the fault current, but also recover the voltage at a permissible level. Hence it keeps the PV system to be connected to the grid.
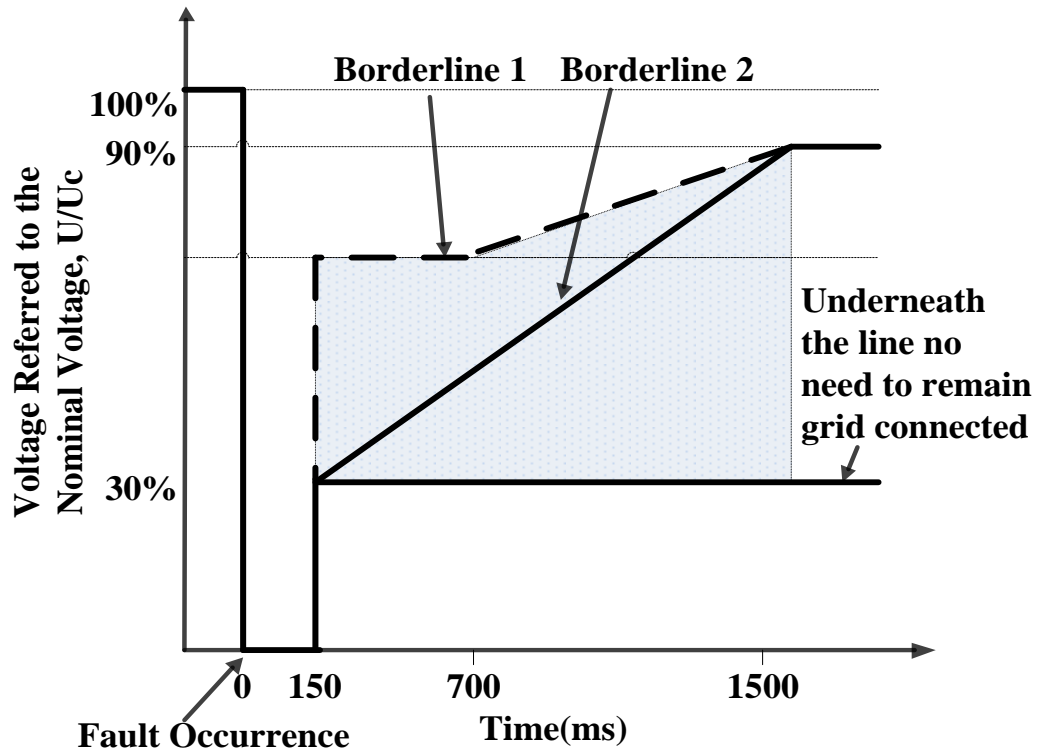
Figure 26. Limiting curves of voltage at the grid connection point for a generating facility of type 2 in the event of a network fault [32][42].
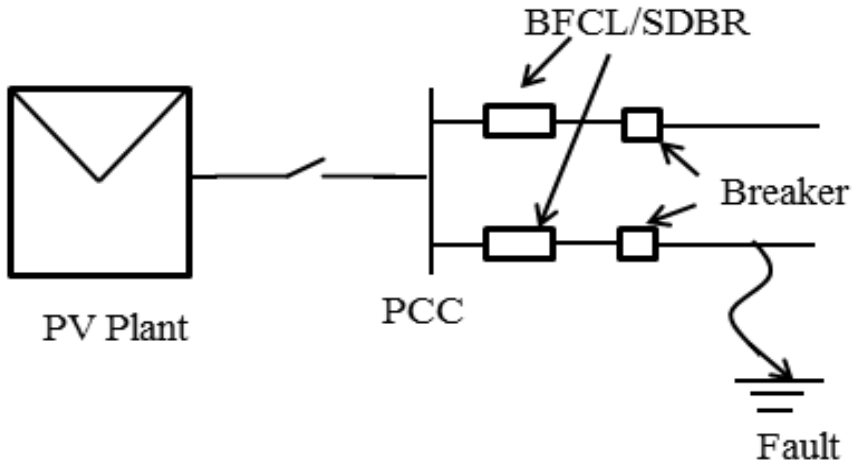
Figure 27. Position of the BFCL/SDBR.

B. *Voltage Sag Study at the Connection Point of PV*

This section discusses briefly about voltage sag since the proposed methods deal with voltage sag improvement and hence enhancement of the LVRT capability of the PV plant. Voltage sag depends on short-circuit current value at the time of fault occurrence. An effective approach to prevent expected voltage sag and improve the voltage quality of point of common coupling (PCC) is fault current limitation by means of a device connected at the beginning of most exposed radial feeders [38]. A simple voltage divider is employed to calculate the voltage sag in [21]. Figure 28 shows the single-line diagram of PV plant connected to the PCC. Equation 12 represents the magnitude of voltage sag at the PCC during the period of fault. In case of fault, Z_F is equal to zero approximately [38]. Therefore, at this condition, the PCC voltage will be approximately zero and this will disconnect the PV plant according to the grid code. Sudden tripping of a big PV plant is undesirable considering the power system stability. If the voltage sag can be prevented, then the disconnection of the PV plant can also be prevented. To prevent the voltage sag, a proper solution is to introduce impedance between the PV plant PCC and the fault point. In this work, the DBSR and BFCL are employed to serve this purpose.
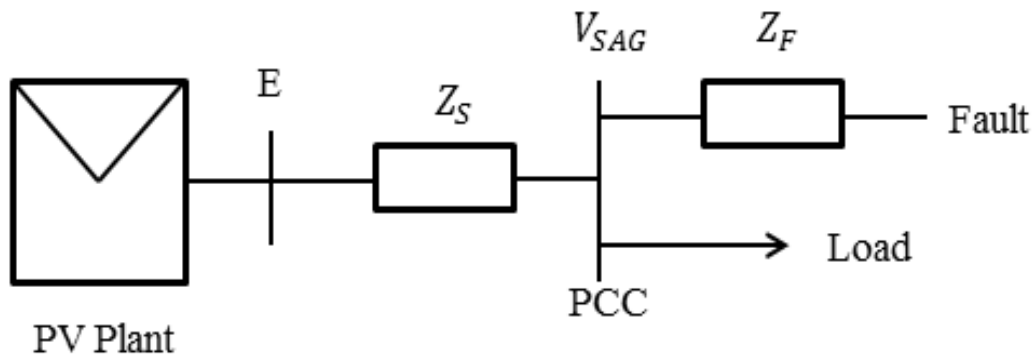
Figure 28. One line diagram of grid connected PV.

$$V_{SAG} = \frac{Z_{IMD}}{Z_F + Z_S} E \qquad (19)$$

Where V_{SAG} is the voltage magnitude at the PCC with the appearance of the fault in the line, $Z_{IMD} = Z_F + Z_{BFCL/SDBR}$, Z_S is the source impedance and E is the magnitude of the source voltage.

C. BFCL and SDBR Control Strategy

a. BFCL

Figure 29 shows the bridge type fault current limiter (BFLC) [38]. It consists of two branches: bridge part and shunt branch. The bridge part consists of a diode rectifier bridge, a small dc link reactor (L_{dc}) connected to a very small series resistor, a IGBT/ GTO based semiconductor switch and a freewheeling diode (D_5) [38]. The shunt brunch consists of a resistor and an inductor ($R_{sh} + j\omega L_{sh}$) which is employed as the compensator. In this work, the value of R_{sh} and L_{sh} are considered as 100Ω and $0.1H$, respectively and the bridge parameters R_{dc} and L_{dc} were considered as 0.3Ω and $5mH$, respectively. Since the values of R_{dc} and L_{dc} are very low, they have negligible effect at the time of normal operation.

At the time of normal operation, the semiconductor switch remains in the on state and the positive half line current passes through D_1, L_{DC}, semiconductor switch and D_4. For the negative half cycle, current conduction takes place in D_3, $L_{DC,}$ switch and D_2. L_{DC} imposes negligible voltage drop at the time of normal operation.
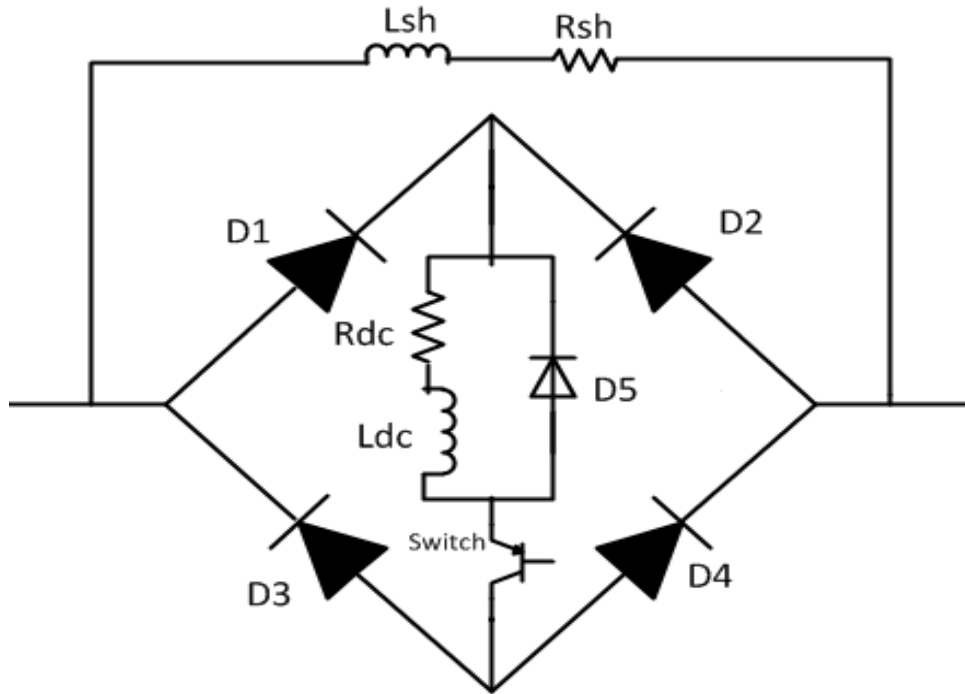
Figure 29. Bridge type FCL [38].
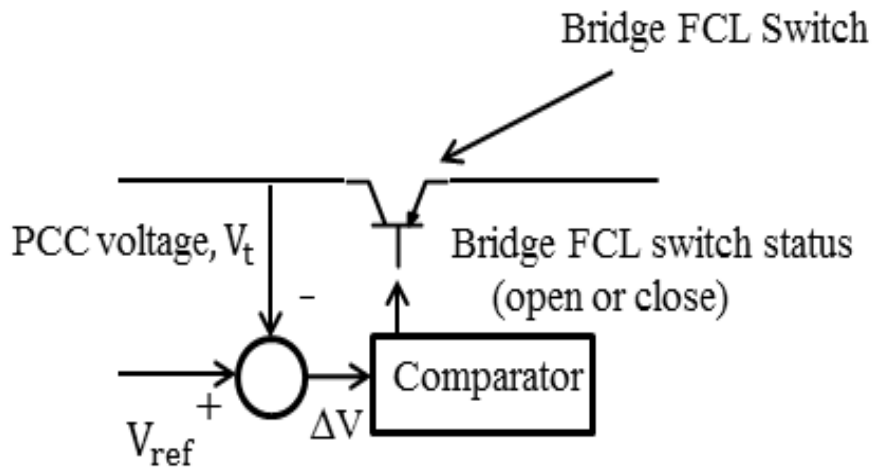
Figure 30. Control scheme of BFCL.

Figure 30 represents the control scheme of the BFCL. When the fault is appeared on

the feeder line, the PCC voltage goes low. According to the proposed method, if ΔV

(difference in voltage) is positive, then the semiconductor switch goes to off state and the

shunt impedance come into action with faulted line, while if ΔV is negative or zero, then

the switch is closed and goes in normal operation. This impedance limits the fault current

to the acceptable limit. At the same time the freewheeling diode (D_5) gives the discharge

path when the IGBT switch turns off.

b. SDBR

In this work, series dynamic braking resistor (SDBR) is also proposed to improve the

voltage profile during the fault period. The occurrence of the fault at the grid makes the

inverter incapable of delivering power generated by the PV source due to drop in the grid

voltage. This excess power causes the DC link voltage to go high due to the power

imbalance between the grid side and PV side. The BR concept is employed to contribute

directly to the balance of active power during a fault. It can be done by dynamically

inserting a resistor between fault point and the PV terminal, increasing the voltage at the

connection point of the PV and thereby preventing the DC link voltage to go high

sharply. In this process, the PV needs not to be disconnected immediately from the grid at

the occurrence of the fault.
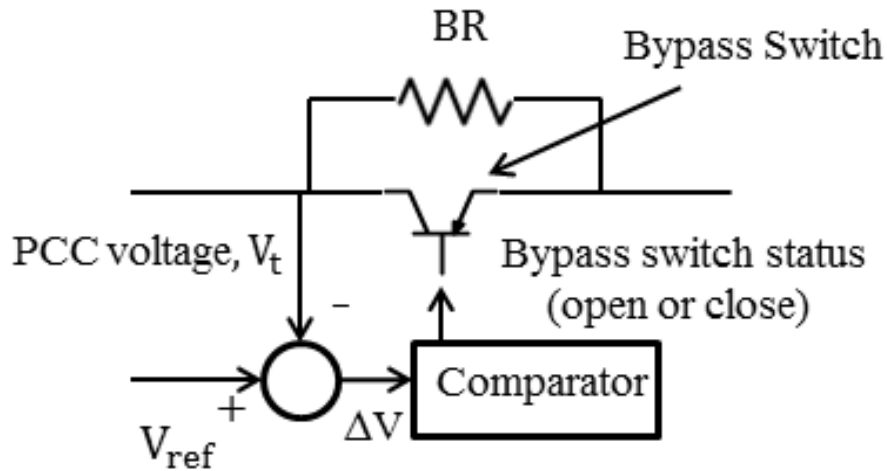
Figure 31. Control scheme of SDBR.

The BR would operate with its parallel switch closed under normal conditions,

bypassing the braking resistor. Voltage depression below a selected set-point would lead

to near-instantaneous tripping of the switch. Current would then flow through the inserted

resistor dissipating power. The proposed braking resistor would remain in the circuit as

long as the PCC voltage of the PV generator is below a threshold value. When the fault is

cleared, the system becomes stable and the PCC voltage becomes same as the reference

voltage, the switch would close and the circuit would be restored to its normal state.

Figure 31 shows the control methodology of the proposed braking resistor. According to

the proposed method, if ΔV (difference in voltage) is positive, then the bypass switch is

open, while if ΔV is negative or zero, then the bypass switch is closed. Thus a closed

loop control of the proposed braking resistor is realized.

D. Simulation Results and Discussion

In this work, all the simulations are performed through Matlab/Simulink software.

Simulations have been carried out considering the severest fault (3LG: three-phase-to-

ground) at F_1 location as shown in Figure 32. The fault is considered to occur at 1.1 sec, the breakers of the lines are opened at 1.18 (5 cycle) sec and reclosed at 2.01 sec (50 cycle). A simulation time of 4sec with 1µs time step is considered. All the simulations are carried out under variable irradiance and constant temperature (25^0 C).The major contribution of this work is two folds, namely DC link overvoltage protection and enhancement of LVRT of PV plant by improving the voltage sag at the point of common coupling.

Figure 32 shows the inverter DC link voltage profile with no protection and also with BFCL and DSBR. Without any grid fault or disturbance in the grid side the normal inverter DC link voltage is maintained at 1000V. In case of 3LG fault at grid side, the DC link voltage goes at a voltage level about 2000V sharply (about 200% of the nominal voltage). This would cause damaging of the inverter circuit and also can isolate the PV generation plant. The reason is that, when a fault occurs, the inverter is unable to deliver power generated by the PV plant to the grid because of the drop in the grid voltage. The excess energy gives a sharp rise to the DC link voltage. But, with the individual protection of BFCL or SDBR, the DC link voltage overshoot is slightly above 101% as shown in Figure 32. Therefore, it is a very effective approach for the DC link overvoltage protection.
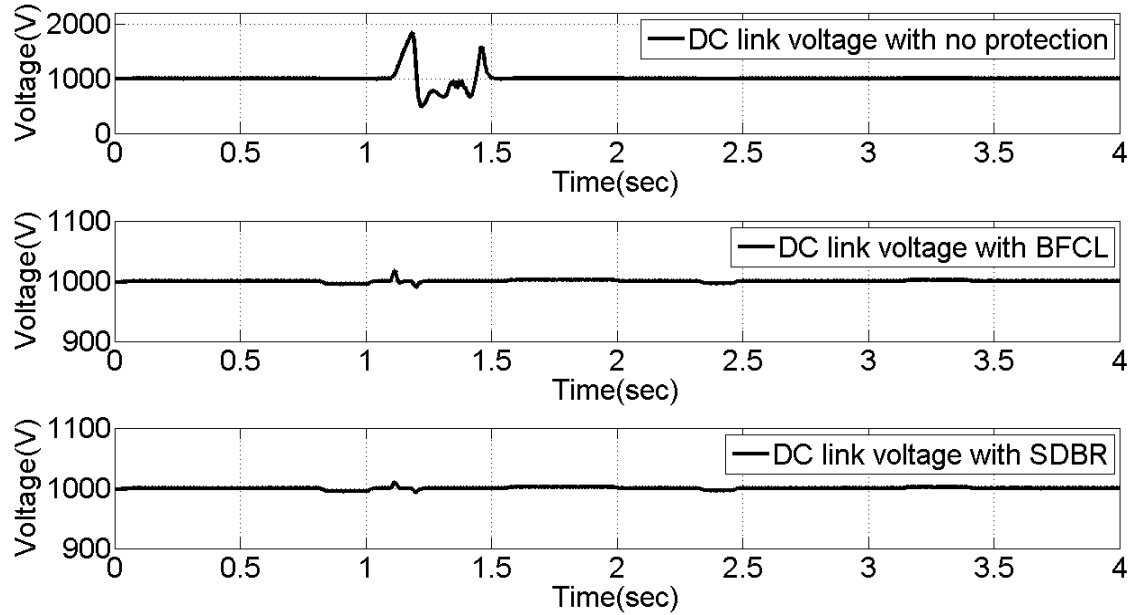
Figure 32: DC link voltage: top one without any protection, middle one with BFCL, and bottom one with DSBR.

A comparison of terminal voltage (connection point of the PV plant to the grid) for no grid side fault protection, protection scheme with BFCL and SDBR are shown in Figure33. For making comparison between the result of the proposed protection schemes and the existing grid code, the terminal voltage is represented in per unit. It is seen that, without any protection, the terminal voltage of the PV plant is zero with the occurrence of the 3LG fault at F_1 point of Figure 20. This would result in disconnection of PV plant in less than six cycles or 0.1 sec according to Table IV. Also, there is a transient situation appeared in the voltage profile after the breaker opening. However, with the proposed protection schemes, the terminal voltage is raised above 0.6pu during the 3LG fault. Therefore, PV would not be disconnected from the grid immediately after the occurrence of the fault. Being the series devices, both the BFCL and SDBR, come into the operation immediately after the fault initiation. Figure 33 shows the actual voltage at the terminal

41

without any protection and with BFCL and SDBR. Actual voltage profile between 1sec

and 1.3 sec is shown, since there is no change in voltage for the rest of the duration. It is

seen from Figs. 33 and 34 that the terminal voltage returns to the nominal voltage

according to the grid code discussed in the thesis.

A comparison of duty ratio with no grid side fault protection and with protection by the

BFCL and SDBR devices are shown in Figure35. In case of no protection during fault,

the duty ratio oscillates since there is no control against the fault. Change in the inverter

DC link voltage at the time of fault causes the duty ratio to be affected. However, with

the BFCL and SDBR the duty ratio is not affected.
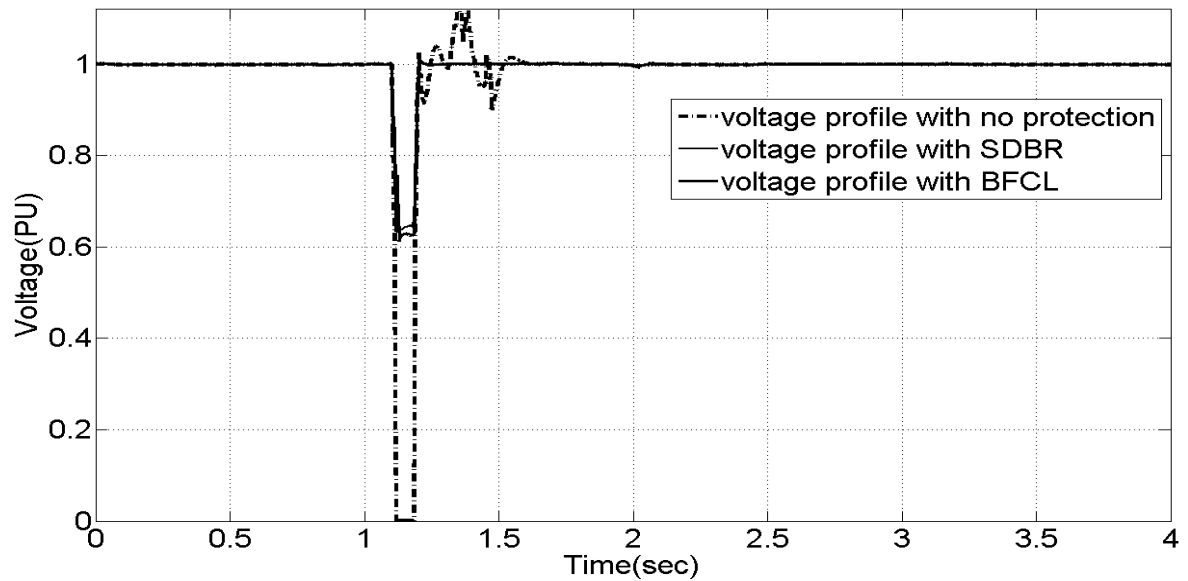
Figure 33. Grid voltage profile with no protection and proposed protections scheme.
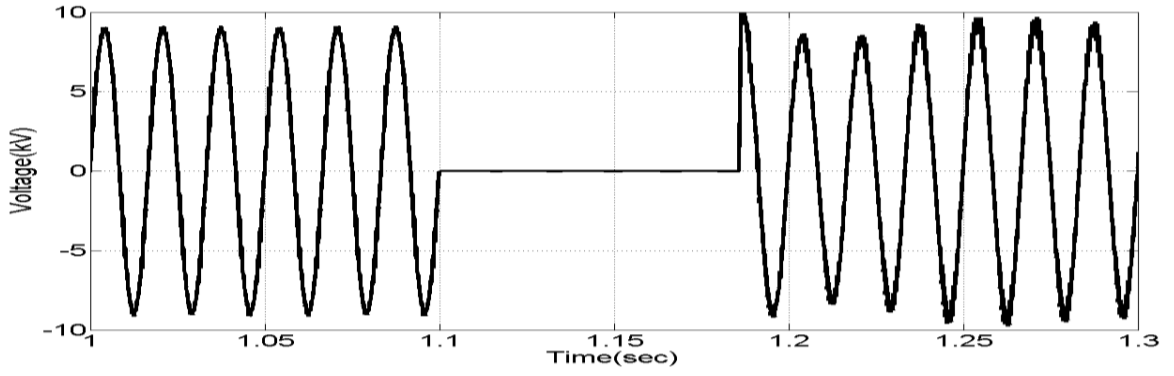
(a)
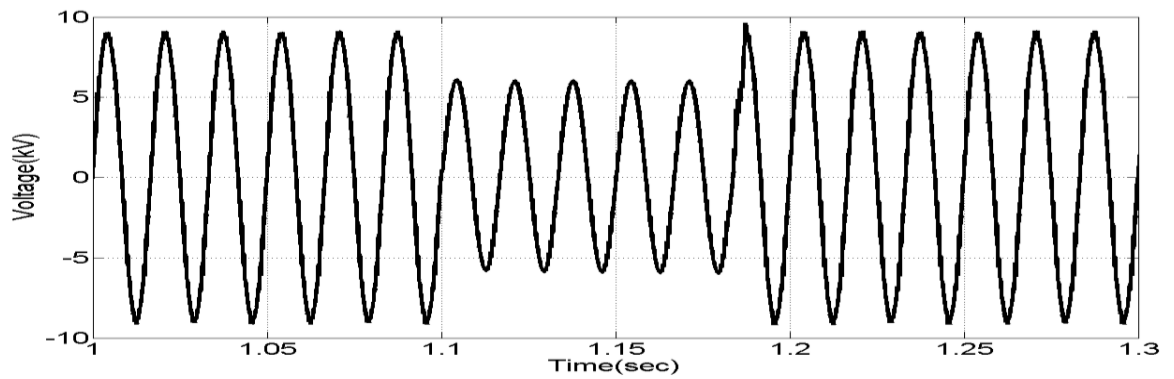
(b)
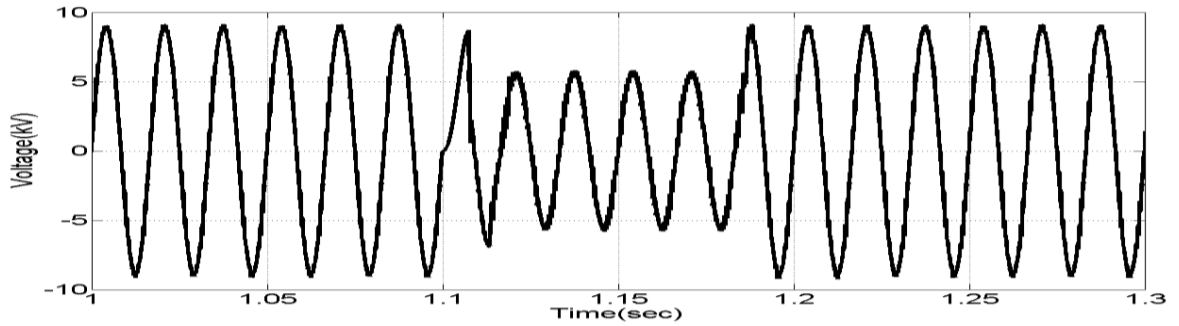
(c)

Figure 34. Actual terminal voltage of PV at PCC with (a) no protection, (b) SDBR, (c) BFCL.
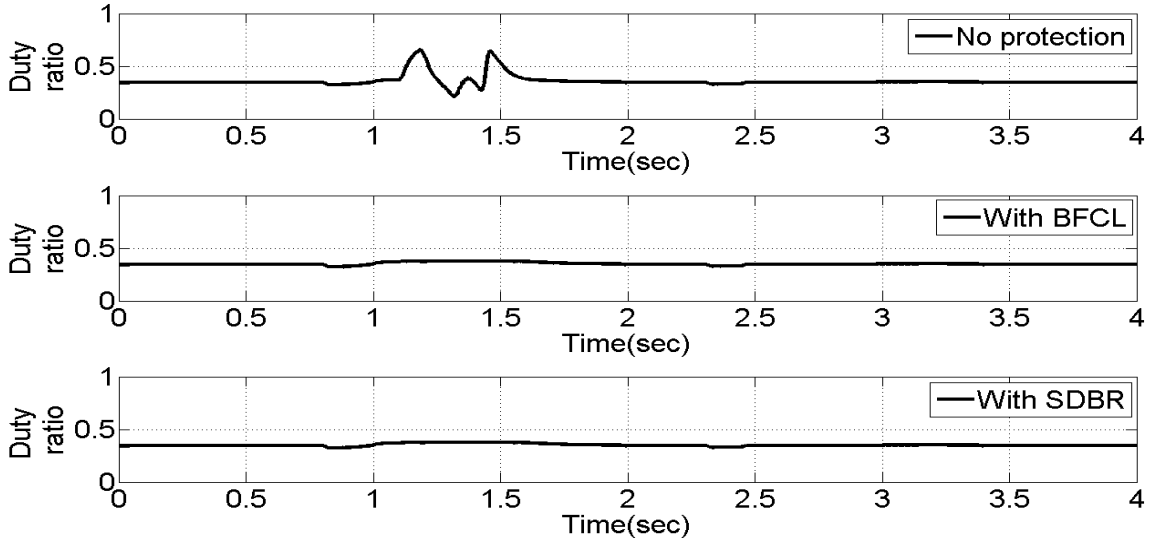
Figure 35. Duty ratio: top one without any protection, middle one with BFCL, and bottom one with DSBR.

Figure 36(a) and 36(b) show the total real power dissipation in BFCL and SDBR, respectively, for 3LG temporary fault at position F_1 in Figure 20. It seen that both the devices are active at the time of the fault occurrence. When the fault occurs in the grid side, the BFCL or SDBR comes into the action and dissipates real power to make the power balance. After the clearance of the fault they are removed from the system by the controller. The amount of power dissipation in SDBR is greater than that of BFCL. Power dissipation in both of the devices depends on the selection of the resistance value.
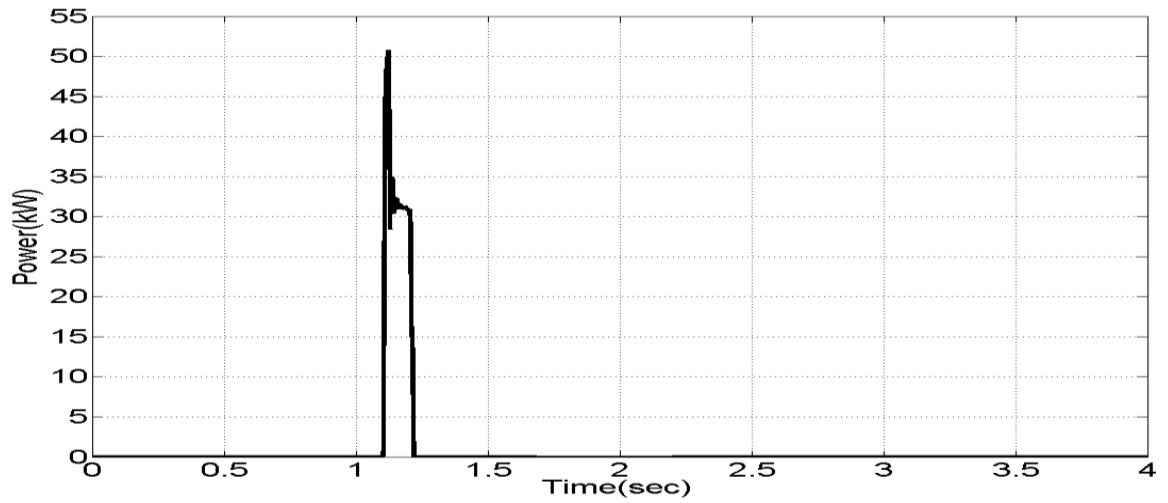
(a)
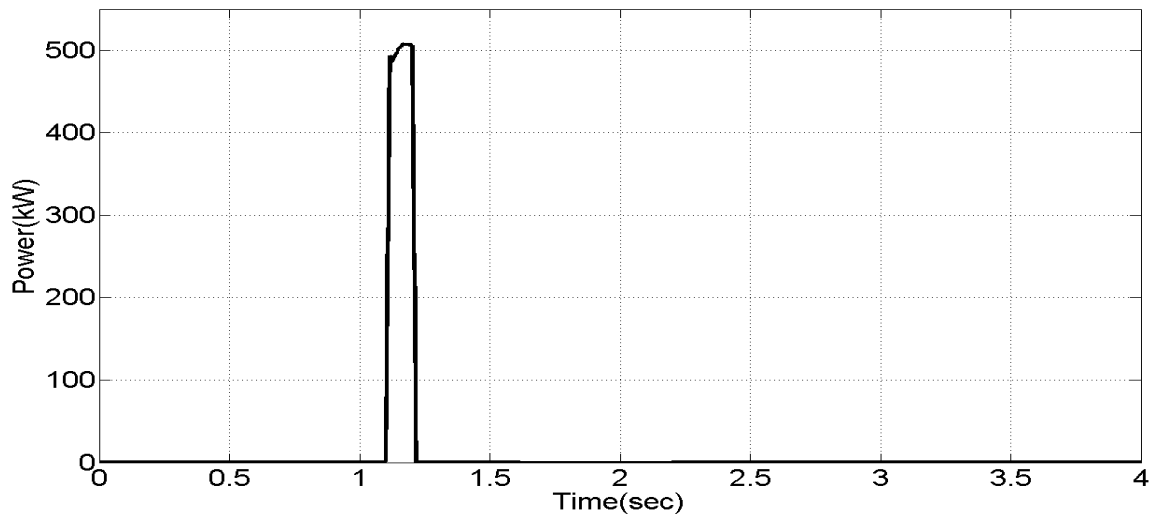
(b)

Figure 36. Real power consumption by (a)BFCL and (b)SDBR during fault period.

E. Cost Effectiveness

Although we are interested in knowing the cost of both the BFCL and SDBR, but their actual cost is not known. However, from the number of components used in both devices, it can be said that the SDBR may be cheaper than the BFCL. The BFCL consists of passive element like resistor, inductor and capacitor and power electronic switches like IGBT or GTO. However, the SDBR consists of only a linear resistor. Furthermore, the BFCL does not require any cooling mechanism as it does in other superconducting fault current limiter (SFCL). The cryogenic cooling is required for other SFCL technologies, which is very costly. Comparing between the SDBR and BFCL, the performance of the SDBR is better than that of the BFCL. However both of the devices can be implemented commercially, and they can be employed to grid connected PV applications.

IV. SMOOTHING OF FLUCTUATING PV POWER BY DIVERSLY LOCATED PV PLANT

A. *Introduction*

Renewable energy sources such as photovoltaic (PV) and wind have attracted the special attention due to their sustainability and their minimum impact on the environment. These energy sources are environment friendly since they neither produce waste nor pollute air and they are omnipresent. So they can be employed as diverse power harvester to replace primary and conventional fossil fuel (e.g. coal, gas etc) based energy sources. Although the renewable energy sources have these desirable characteristics considering the current environmental protection schemes, they are time varying in nature and produce variable output. The solar irradiance variability is one of the major obstacles to the large scale deployment of solar power generation. Their intermittent power production is undesirable in the context of integration to the conventional power grid.

Currently, PV plants are allowed to integrate with the power grid unless any grid code is violated due to the PV power integration [43]. Considering this case, PV system owners might be requested to adopt the required strategy to smooth out the PV power or they might be asked to restrict their generation to a certain limit [43].

Much research has been conducted since 1980s to determine the impact of solar insolation variability on PV power generation and also the possible impact on grid operation due to the integration of the generated PV power [44]. Some studies demonstrate that PV power output variability decreases from systems at varying levels of spacing [44]. Recently considerable progress has been made in characterizing the

47

smoothing effect. A relationship between the correlation of variability between spatially

diverse PV plants and the resulting aggregate variability of these plants is established in

[45] . The authors in [46] and [47] employ this relationship and present methods for

estimating aggregate system variability from the variability of a single system [44].

Authors in both papers (i.e. in [46] and [47]) state that, for a group of independent PV

plants with similar capacity and variability characteristics, the total variability of systems

will approximate $1/\sqrt{N}$ of the variability of a single site, where N equals the number of

sites [44]. Although, these works were able to show that reduction of the variability is

possible after aggregation, still there might be variation of power. The existing variability

of power may cause the deterioration of power quality when integrated to the grid. In

[48], it is shown that the total output power of 100 PV systems dispersed throughout

Germany fluctuates by small percentage. Figure 37 represents the normalized power

output in a three days period of an individual PV system and the ensembles of 100 PV

systems, which is taken from [48]. It is seen from the figure1 that still there is the

presence of power fluctuation.
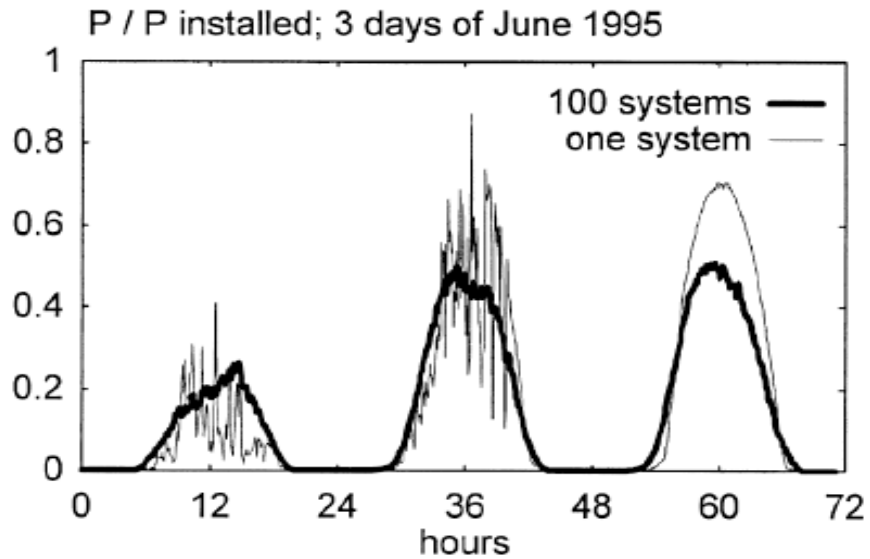
Figure 37. Significant decrease in PV power fluctuation (P/Pinstalled) from 100 geographically distributed PV sites compared to a single PV system [48].

The main focus of this particular work is to propose a methodology to minimize power variability by the aggregation technique and also mitigate the above mentioned existing variability in power with the help of small battery energy storage system. The energy storage system (ESS) is used for removing the PV power variability [49] [50] [51]. In those works since only the EES was used as buffer, the capacity of the EES required was high. The capital and maintenance cost of large capacity energy storage system is a barrier to the large-scale installation of PV systems. But in this work, it is shown that after the integration of distributed PV power, the energy storage size is considerably reduced. Elimination of massive storage device has several advantages, such as, 1) maintenance and replacing cost will be reduced; and 2) the cost for EES can be used for setup extra solar cell in the system.

49
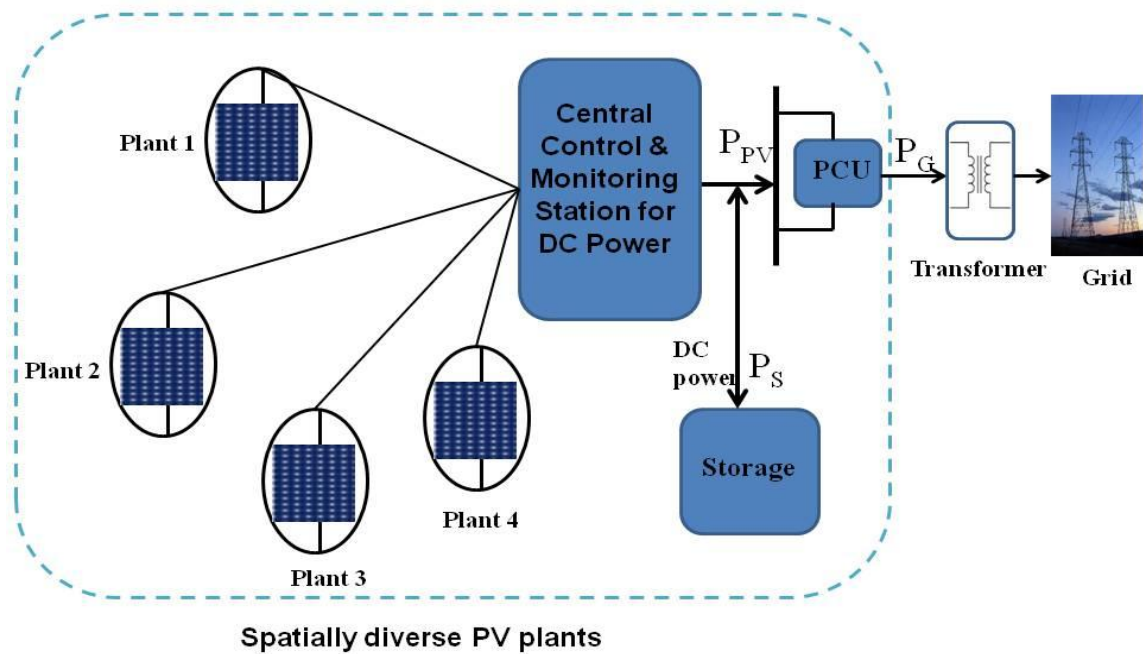
Figure 38. Grid connected spatially diverged PV plants.

Figure 38 represents the spatially dispersed PV system connected to the grid. Only four

PV plants are showed there. But, number of PV plants may be ten, twenty or even more.

The function of central control and monitoring station is to aggregate and control the DC

power. Central control and monitoring station is followed by PCU blocks, where PCU

stands for power controlling unit and the function of this unit is to convert the DC power

into ac power in order to feed the power to the grid. P_{PV} is the dc power from the

diversely located PV plants, whereas P_S and P_G are the power from/to the storage and

power to the grid, respectively. The role of the storage device in figure 39 is to further

smooth the output power of PV system. The energy storage device should have some

characteristics such as its response time should match with the speed of the power

fluctuations and it should be able to provide the energy over the range of few minutes to few hours [52]. There are some advantages in the proposed method:

1) In [48], since 100 different power electronic interfaces are required to integrate the power from 100 different PV stations to the grid and this will cause harmonics insertion to the grid. Since our proposed method exploits DC power integration of several PV systems first and then the integrated power is injected to the grid it requires less number of power electronic interfaces and less insertion of harmonics to the grid.

2) In this proposed system, DC transmission loss is neglected at the time of integration in a particular point since we are not considering a very large area. Since the proposed method uses DC transmission for PV power integration, the voltage drop will be low compared to the ac transmission voltage drop. The voltage drop for DC transmission line $V_D= IR*cos\theta$, whereas for AC transmission line $V_D= I(R*cos\theta+X*sin\theta)$, where, $cos\theta$ is the power factor [53]. From these two equations it is seen that voltage drop in DC transmission is lower than that in AC transmission.

3) In the figure 38, it is seen that the energy storage system is placed after the integration of the DC power and hence the power fluctuation is minimized already due to distributed PV system. Therefore, we can use only one small energy storage device for multiple PV systems to remove the still remaining power fluctuation. This is advantageous because in this process we can replace the large scale energy storage, which requires frequent maintenance and replacing cost and the residue of this energy storage chemical is hazardous for the environment. Although it is required to bear the extra cost for DC transmission line, but if the distributed PV system is setup for once then it will provide the power for a long time with minimum maintenance cost. Moreover the

DC transmission lines can be placed together with the conventional AC transmission line

with little modification of power line tower.

4)   In the proposed method, the energy storage system is placed with DC bus directly.

If SMES (Superconductive magnetic Energy Storage) [54] or supercapacitor is used as

the EES then the number of componenets required to set up these EESs are less. For

example, if small capacity SMES is used as the EES then transformer and volatge source

converter (VSC) are not required and thus the complexity of the SMES is reduced in the

proposed system. Figure 39 repesents the use of SMES with the proposed system and

conventionl system.
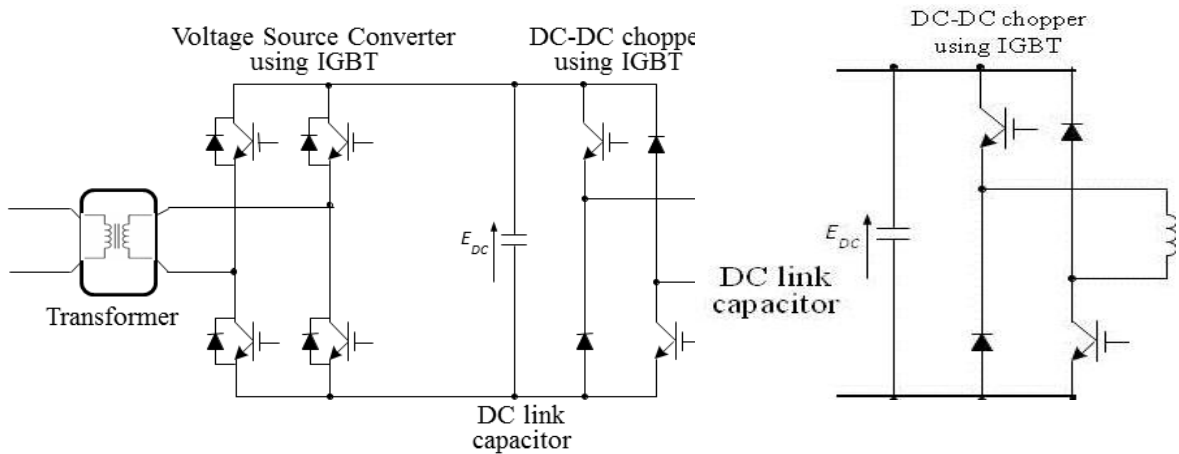
Figure 39. Use of SMES with (a) conventional power system, (b) proposed spatially
dispersed PV system [54].
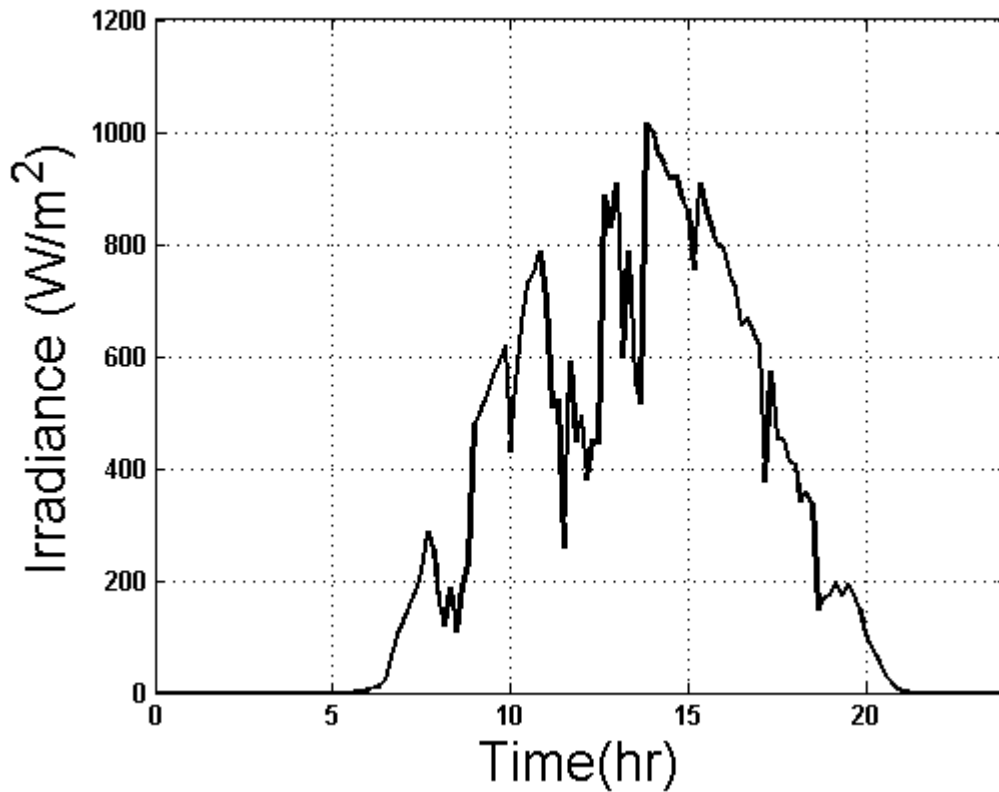
Figure 40. Irradiance profile of a particular day.

Figure 40 represents the irradiance profile of a particular day measured by the

insolation measuring instruments (Payranometer). It is seen from the above irradiance

profile that the irradiance is varying in nature. Since PV power dependent on irradiance,

it will also be varying in nature. However, integration of varying power to the grid causes

different types of power quality problem such as frequency and voltage variation.

If the small PV stations are located spatially diverged instead of a big equivalent PV

power plant in one point, then after adding the irradiance data collected from different

stations smoother irradiance curve can be obtained. The reason is that, at a particular time

one PV station might be partially blocked by cloud and the other remotely located station

may not have any cloud effect at that time, then one plant compensates another PV plant's irradiance deficiency.

In Figure 41 it is shown that averaging the irradiance data of multiple spatially dispersed PV plants does in fact reduce the variability of the solar irradiance and leads to a smooth irradiance curve. In Figure 41(a), five stations irradiance data and their average are plotted together. The average irradiance curve of five stations still has some fluctuation. But in Figs. 41(b) and 41(c), 10 and 20 stations irradiance data as well as their average are plotted respectively, and it is seen that as the number of stations are increased the average irradiance fluctuations are reduced. The bold blue line is the average irradiance data in Figure 41 and it is seen that 20 stations data can produce smoother curve than 10 and 5 stations data. The idea of averaging the irradiance data for spatially dispersed PV station is helpful for understanding the smoothing effect. Since PV power varies with solar irradiance, this smoothing effect is also applicable for output PV for spatially dispersed PV plants.
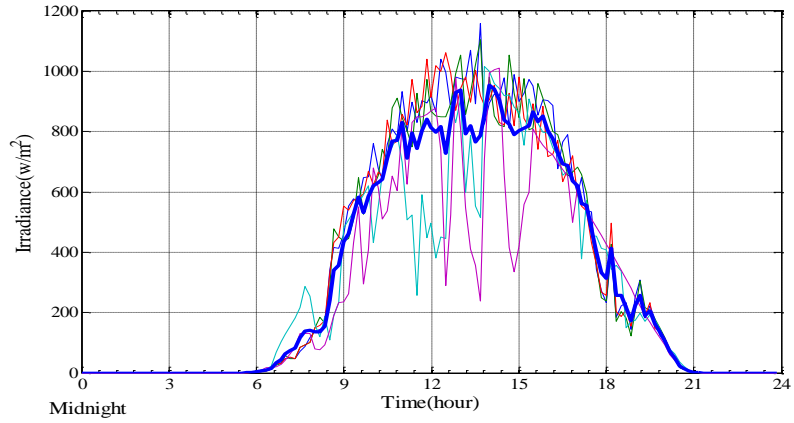
(a)
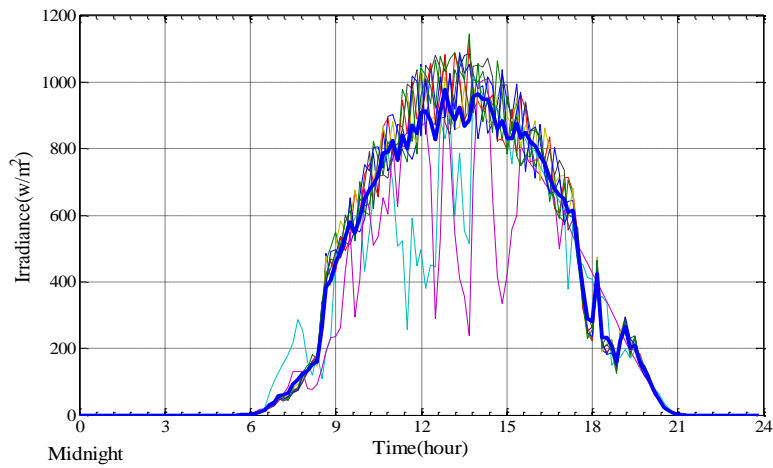
(b)
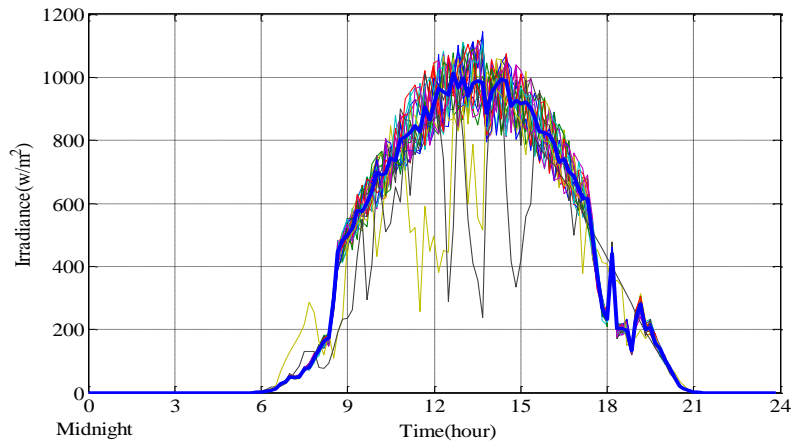
(c)

Figure 41. Irradiance plot. (a) Irradiance plot of 5 PV stations and their average, (b) Irradiance plot 10 PV stations and their average, (c) Irradiance plot of 20 stations and their average.

D. Conversion of Irradiance Data to the PV Power

Using the solar irradiance, the power output of the PV generator, $P_{PV}(t)$, can be calculated according to the following equation [55]:

$$P_{PV}(t) = Ins(t)AEff_{pv} \qquad (20)$$

where $Ins(t)$ is the irradiance data at time t (W/m^2), A is the area of a single PV panel (m^2), and Eff_{pv} is the overall efficiency of the PV panels and the DC/DC converter.

E. Smoothing Effect of Power Curve

After converting the irradiance data to the PV power, they are added together to see the smoothing effect for spatially dispersed PV system. Figure 42 represents the smoothing effect. It is shown in Figure 42(b) that when only five stations are integrated together, the cumulative power has some fluctuation. But, when ten stations are integrated together the fluctuations are less as compared with the previous five PV integrated system. Thus, the power in Figure 42(d) has less fluctuation than that of in Figure 42(b). Finally, we considered 20 PV stations and we integrated them together and we get the best PV power in terms of less fluctuation. The integrated PV power from 20 spatially dispersed PV stations is shown in Figure 42(f), whereas, Figure 42(e) represents the power plot of individual 20 PV stations. It is seen that the cumulative power for the 20 PV station has still some fluctuation. Since the power quality is influenced by still existing power fluctuation, we proposed a method for reducing the still existing power fluctuation with the help of energy storage system.

(a)

(b)

(b)

(d)

(d)

(e)
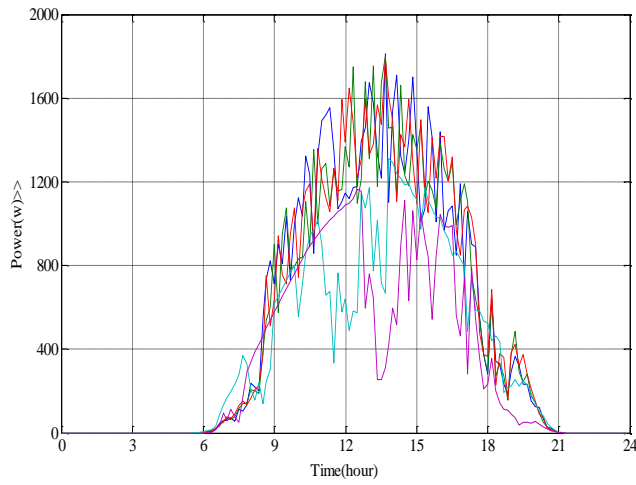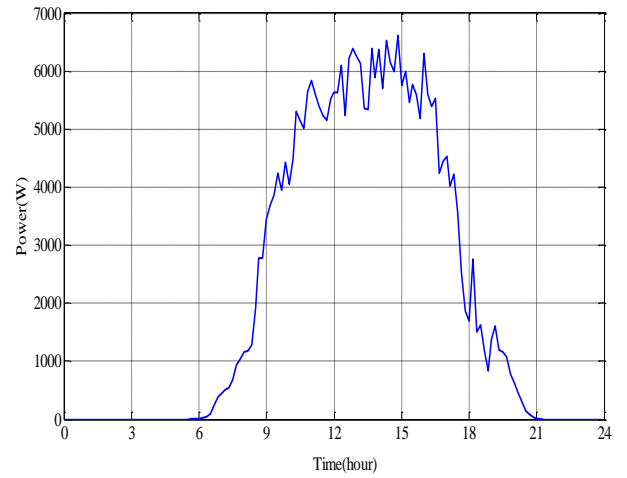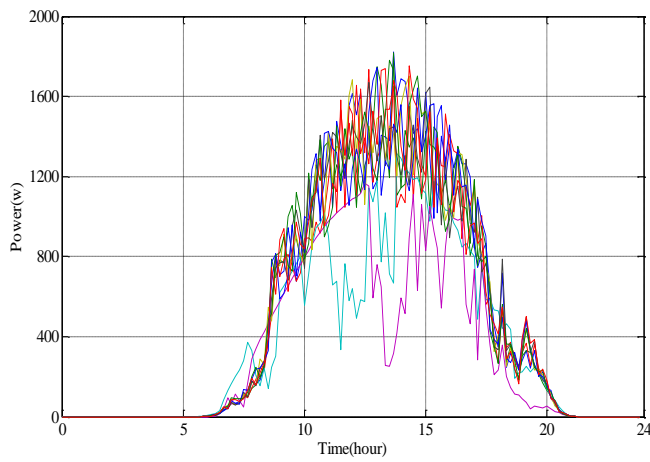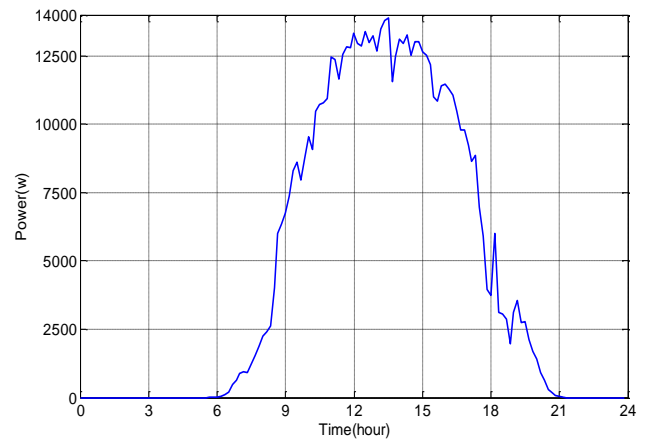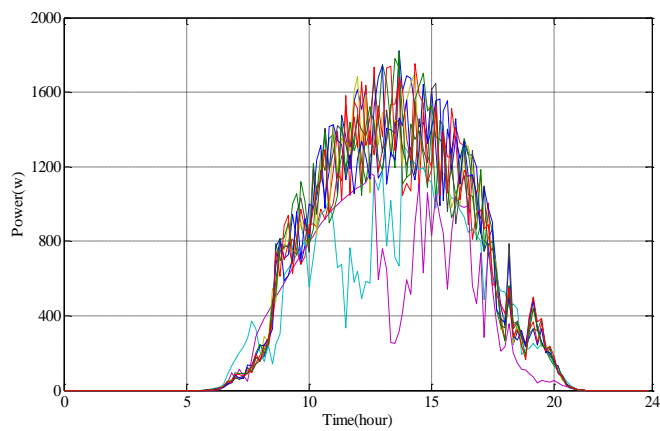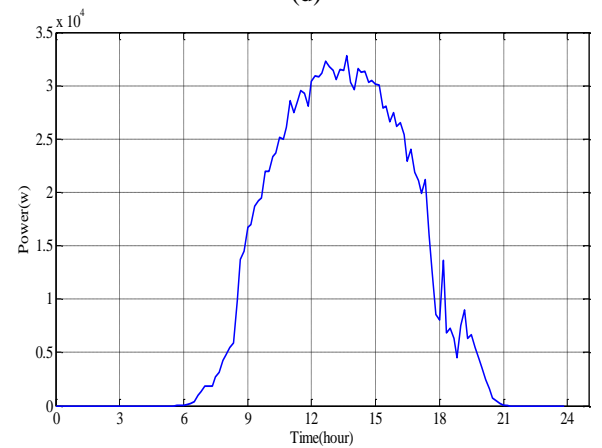
Figure 42. Power plot. (a) 5 PV stations together, (b) Integrated PV power of spatially dispersed 5 PV stations, (c) 10 stations together, (d) Integrated PV power of spatially dispersed 10 PV stations, (e) 20 stations together, (f) Integrated PV power of spatially dispersed 20 PV station.

F.   Further Smoothing by Small Capacity Energy Storage

The function of energy storage device in PV power applications are bridge pwer fluctuation, outage protection and shifting the peak generation period [56]. A variety of storage technologies are available in the market like battery energy storage systems (BESS), ultra capacitor or super capacitor, flywheel, pumped storage hydroelectric systems, and superconducting magnetic energy storage (SMES) systems [54]. Battery energy storage systems are perceived as the effective energy storage system for Pv applications Due to large energy density and fast access time [57]. Some of the disadvantages of BESS include limited life cycle, voltage and current limitations, and potential environmental hazards [54]. Ultra capacitor or super capacitor is an emerging device for energy storage and it is employed in [56] for PV power application. Both electric utilities and the military have exploited SMES systems and it has attracted the attention due to fast response and high efficiency (a charge–discharge efficiency over 95%) [36]. Most of the above motioned energy storage techniques are already implemented in PV power application.

Adopting a strategy of smoothing the fluctuating PV power by aggregating and then further smoothing by small scale energy storage will make the PV power direct dispatchable to the grid. Due to direct dispatch to the grid there is no need for storing the energy at large-scale and this will reduce the system cost, since there is no need for large-scale energy storage. This section investigates the use of energy storage system with spatially dispersed PV stations.

Figure 43 illustrates the use of energy storage to compensate the small power output fluctuation of the spatially dispersed PV firm. The energy storage system is connected to

the system at the point of common coupling and is charged/discharged through a power

converter to smooth the net power to be injected to the grid.
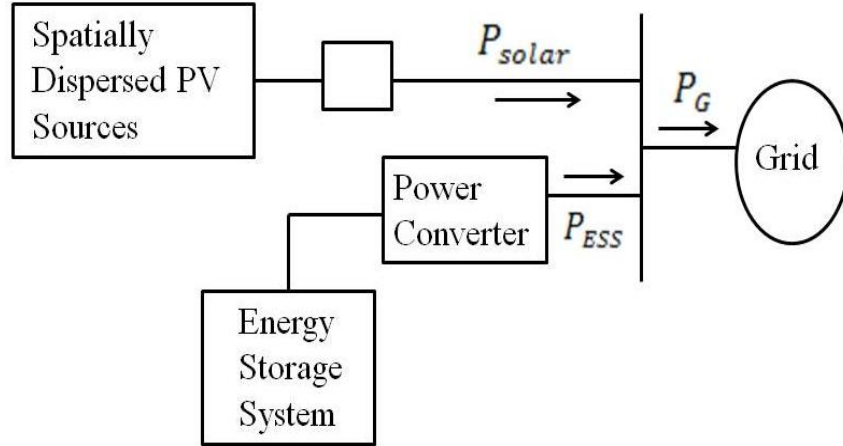
Figure 43. Smoothing of Spatially Dispersed PV power with Small
Capacity Energy Storage.

G.   *Comparison of Energy Storage Needed for Diversely Located PV System and an*

       Equivalent Big Plant

   For smoothing purpose energy storage is required, and in this section, a comparison is

presented between the energy storage needed for a big PV station at one place and the

other PV system that consists of spatially dispersed small PV plants. It is assumed that

both power stations have the same capacity. For making comparison, a reference is

needed. In this case, the time average of solar power output P_{solar} of spatially dispersed

PV plant can be used as the reference power.

$$P_{reference} = \overline{P_{solar}} \tag{21}$$

where $\overline{P_{solar}}$ is the moving average at time period T and it can be determined by the

following equation [58].

$$\overline{P_{solar}} = \frac{1}{\tau}\int_{t-\tau}^{\tau} P_{solar}d\tau \qquad (22)$$

Figure 44(a) represents the moving average of the spatially dispersed solar power with time and it is used as the reference level. The difference between $P_{reference}$ which is considered as moving average and the estimated solar power P_{solar} is absorbed by the storage system as

$$P_s = P_{reference} - P_{solar} \qquad (23)$$

The energy storage device should have the capacity to absorb the difference and estimating the capacity of the energy storage device is important. Figure 44(b) represents the difference in reference power and solar power.
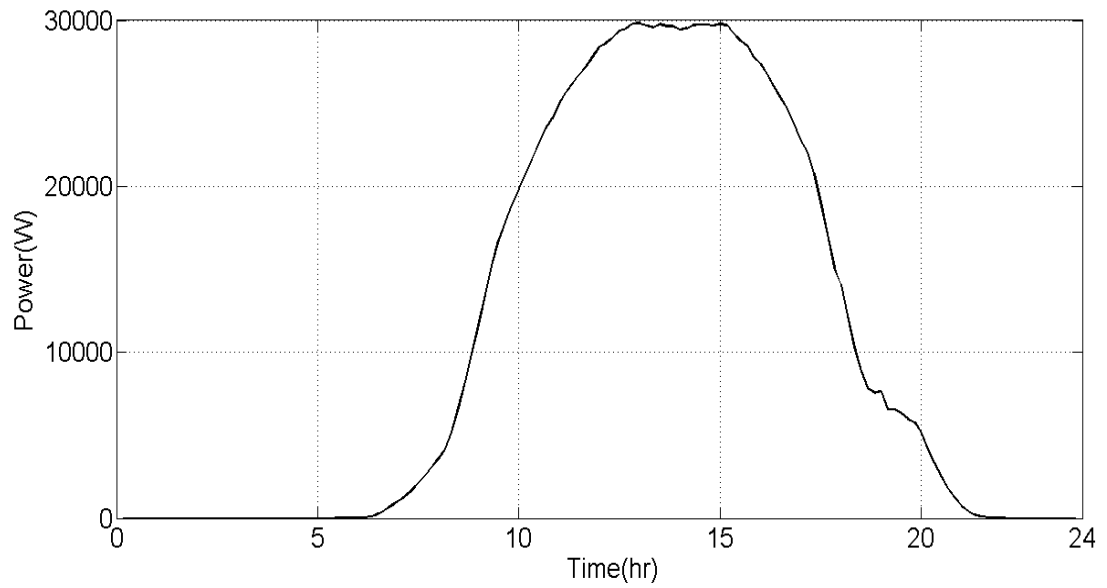
(a)
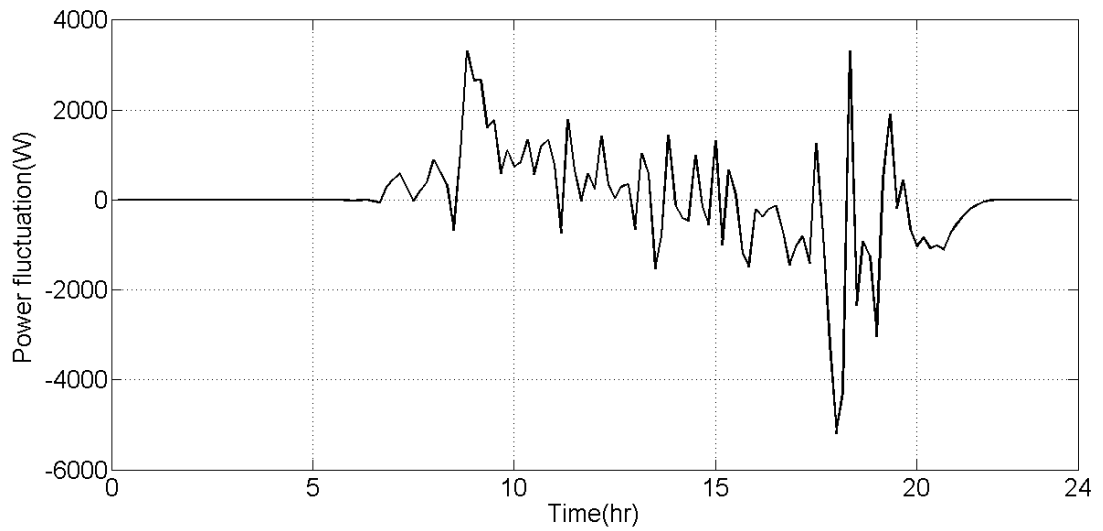
(b)

Figure 44. (a) Moving average (reference power), (b) Preference -Psolar   (in watts).

Instead of using spatially dispersed 20 identical PV plant, if we use one equivalent big

PV plant in a particular area then we will see high power fluctuation. Figure 45(a)

represents PV estimated power for a big PV station equivalent to spatially dispersed 20

PV plants and the reference power together and Figure 45(b) represents the power

fluctuation which will be absorbed by energy storage device. If we want to reduce the

power fluctuation with energy storage, then the size of the energy storage will be big for

one big PV plant. On the other hand, for 20 spatially dispersed PV systems, the

aggregated power has small fluctuation. Therefore, in order to smooth out this small

fluctuation we need small capacity energy storage.
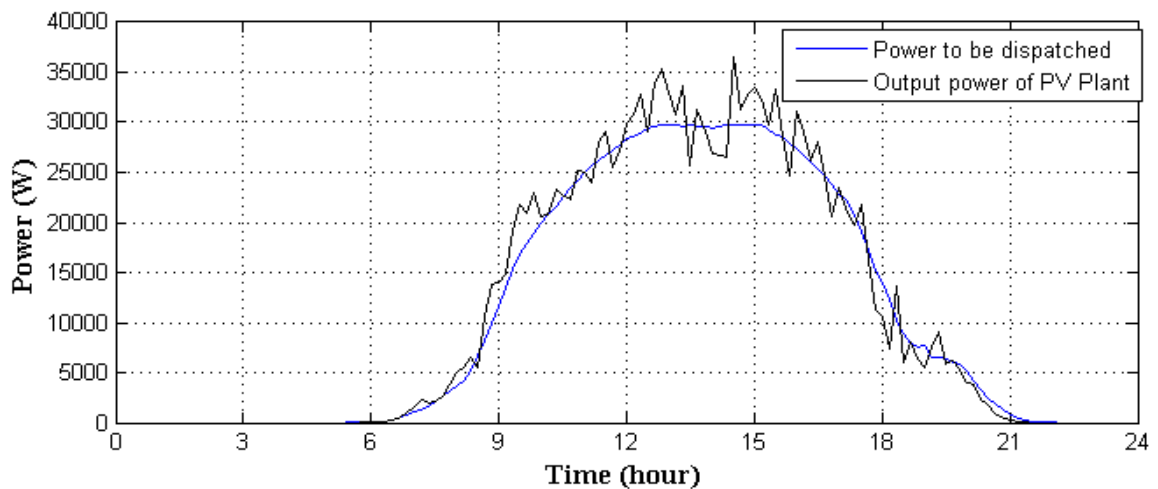
(a)
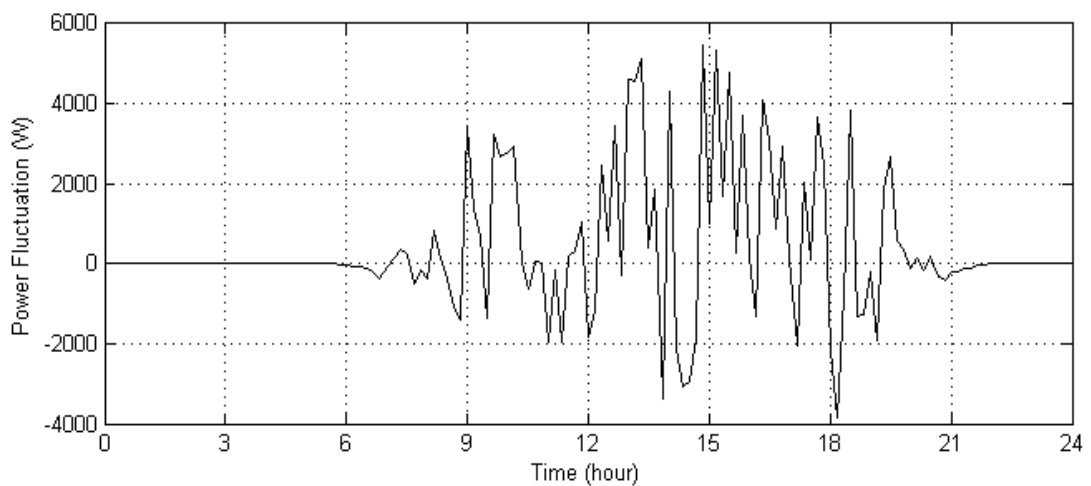
(b)

Figure 45.   (a) Reference power and output power (b) High fluctuation of power for one
big PV plant.

H.   Determining the Size of the Energy Storage

We can also determine the size of the energy storage device for smoothing purpose of PV power in case of both 20 spatially dispersed PV systems and a big PV plant equivalent to spatially dispersed 20 PV plants. The maximum size of the storage device is determined by integrating the charging and discharging power in a particular period of time. Following equation can be used to determine the maximum size of the energy storage.

$$E_{max} = \int_0^t P_s dt \tag{24}$$

Where E_{max} is the maximum size of the energy storage and P_s is the power absorbed (charging or discharging) by the energy storage device.

About 35 kw of maximum capacity was calculated for particular area of the PV plant and then the size of the energy storage needed to smooth out the power fluctuations was calculated for both cases, i.e., spatially dispersed PV systems and an equivalent big PV plant. For spatially dispersed PV system, a maximum size of 52kwh energy storage was calculated. On the other hand, for the same capacity of a big plant the maximum size of the energy storage is 126.83kwh, which is greater than twice the size of the energy storage required to smooth out PV power fluctuation in case of spatially dispersed PV system. Figure 46 represents the energy storage required to smooth out PV power fluctuation in case of spatially diverged PV plant and a big PV plant having capacity the same as the spatially diverged PV plant for existing sunlight period.
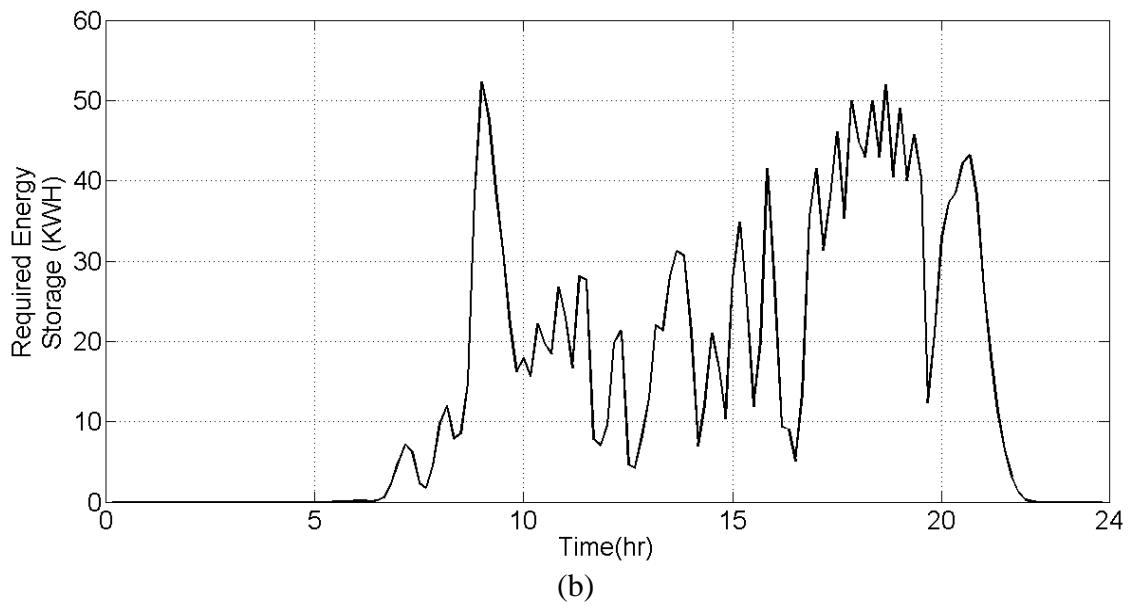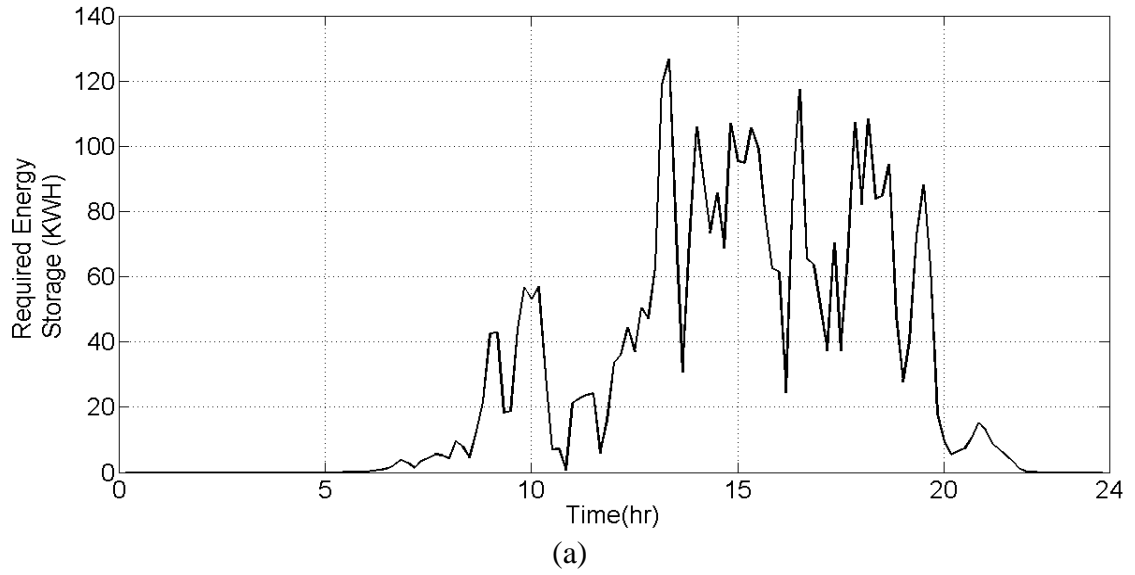
Figure 46. Energy storage required to smooth out PV power (a) for spatially diverged PV plant, (b) a big PV plant with capacity same as the spatially diverged PV plant.

V. CONCLUSION, CONTRIBUTION OF THE THESIS AND FUTURE WORK

A. *Conclusion*

In this thesis, a complete modeling of grid connected PV system is presented. This thesis proposes the application of BFCL and SDBR for enhancing the LVRT capability and inverter DC link protection of grid connected PV system. Penetration of PV power on distribution level is gradually increasing, and the proposed protection schemes for grid connected PV systems might play an important role to grid integration of PV power.

This thesis also presents a method for small scale energy storages to smooth out the outputs of distributed PV units in order to directly dispatch power to the grid. Cases of Multiple distributed PVs and one big equivalent PV plant to the distributed PVs are compared. Based on results, the following points are noteworthy.

1) The proposed methodologies are capable of enhancing the LVRT capabilities of grid connected PV system.

2) DC link overvoltage protection is possible with the proposed protection schemes.

3) Undervoltage tripping of the big PV plant can be prevented by the proposed schemes, as required by the recent grid code.

4) Although, both BFCL and SDBR are capable of enhancing the LVRT capability of grid connected PV system, however, SDBR has simple construction and control complexity than BFCL.

5) Mitigation of PV power fluctuation of diversely located PV plant is possible by the proposed method.

6) Further minimization of fluctuation can be done with the help of small capacity energy storage device.

The size of the energy storage required for the diversely located PV system is smaller than that for a big PV plant. In this work, we estimated the capacity of the PV plant considering the particular area of the plant and then we determined the maximum size of the energy storage required to smooth out the PV power. If the size of the PV plant is varied, then the energy storage required for the smoothing purpose will also vary accordingly.

B. Contribution of the thesis

There are numerous applications of BFCL and SDBR in the power system stability analysis. But there are no works associated with BFCL and SDBR in PV power applications and that is the main and original contribution of this work. Moreover, another aspect of PV power which is smoothig of PV power is investigated in this work.The originality of this work lies in DC integration of PV power to smooth out the PV power fuctuation.

C. Future Work

In future, different types of fault associated with PV such as PV array internal fault and DC link fault will be investigated. The novel protection schemes for these types of PV fault will be investigated. Also, other means of improving low voltage ride through capability will be investigated in the future research. Moreover, a novel control strategy for optimum use of the energy storage system with distributed PV application will be investigated.

VI. Bibliography

[1] M. Fadaee and M. Radzi, "Multi-objective optimization of a stand-alone hybrid renewable energy system by using evolutionary algorithms: A review," *Renewable and Sustainable Energy Reviews,* vol. 16, pp. 3364– 3369, Jun. 2012.

[2] H. Kim, S. Kim, C.-K. Kwon, Y.-J. Min, C. Kim and S.-W. Kim, " An Energy-Efficient Fast Maximum Power Point Tracking Circuit in an 800 µW Photovoltaic Energy Harvester," *IEEE Trans. Ind. Electron,* vol. 28, no. 6, pp. 2927–2925, Jun. 2013.

[3] IEA, "Cost and Performance Trends in grid-connected photovoltaic systems and case studies," *International Energy Agency,* 2007.

[4] Y. Zhao, "Fault Analysis in Solar Photovoltaic Arrays," *M.S. Thesis, ECE. Dept. Northeastern Univ., Boston, MA,* 2011.

[5] EPIA, "Global market outlook for photovoltaics until 2014," *European Photovoltaic Industry Association (EPIA),* 2010.

[6] A. Luque and S. Hegedus, Handbook of Photovoltaic Science and Engineering, Chichester: Wiley, December 2, 2002.

[7] M. G. Villalva, J. R. Gazoli and E. R. Filho, "Comprehensive Approach to Modeling and Simulation of Photovoltaic Arrays," *IEEE Trans. Power Electron.,* vol. 24, no. 5, pp. 1198-1208, May 2009.

[8] [Online]. Available: http://www.bls.gov/green/solar_power/.

[9] "SolarWorld," [Online]. Available: http://www.solarworld-usa.com/about-solarworld/value-chain#Solar_cells.

[10] R. A. Messenger and J. Venture, Photovoltaic System Engineering, Boca Raton: CRC Press Taylor & Francis Group, 2010.

[11] [Online]. Available: http://cyberparent.com/solar-electricity/pv-solar-cells-modules-arrays.htm.

[12] "samlexsolar," [Online]. Available: http://www.samlexsolar.com/learning-center/solar-cell-module-array.aspx. [Accessed 19 september 2013].

[13] Y. Gi, D. Jung, T. Lee and C. Won, "A real maximum power point tracking method for mismatching compensation in PV array under partially shaded conditions," *IEEE Trans. Ind. Electron.,* vol. 26, no. 4, pp. 1001–1009, Apr. 2011.

[14] K. Ishaque, Z. Salam, H. Taheri and Syafaruddin, "Modeling and simulation of photovoltaic (PV) system during partial shading based on a two-diode model," *Simulation Modelling Practice and Theory,* vol. 19, pp. 1613–1626, Aug. 2011.

[15] M. Aureliano, G. D. Brito, L. Galotto, L. P. Sampaio, G. D. A. E. Melo and C. A. Canesin, "Evaluation of the Main MPPT Techniques for Photovoltaic Applications," *IEEE Trans. on Indus. Electron.,* vol. 60, no. 3, pp. 1156-1167, Mar. 2013.

[16] K. Ishaque, Z. Salam and H. T. , "Accurate MATLAB Simulink PV System Simulator Based on a Two-Diode Model," *Journal of power electronics,* vol. 11, no. 2, pp. 179-187, Mar. 2011.

[17] C. Sah, R. N. Noyce and W. Shockley, "Carrier generation and recombination in p-n junctions and p-n junction characteristics," *in Proc. IRE,* vol. 45, no. 9, pp. 1228-1243, 1957.

[18] "KC200GT High Efficiency Multicrystal Photovoltaic Module Datasheet," [Online]. Available: http://www.kyocera.com.sg/products/solar/pdf/kc200gt.pdf.

[19] M. G. Villalva, J. R. Gazoli and E. R. F. F., "Modeling and Circuit-Based Simulation of Photovoltaic Arrays," *Brazilizn Journal of Power Electronics,* vol. 14, no. 1, pp. 35-45, 2009.

[20] M. K. Hossain and M. H. ali, "Overview on Maximum Power Point Tracking (MPPT) Techniques for Photovoltaic Power Systems," *International Review of Electrical Engineering,* vol. 8, no. 3,pp. 1363-1378, Aug. 2013.

[21] N. Femia, G. Petrone, G. Spagnuolo and M. Vitelli, "Optimization of perturb and observe maximum power point tracking method," *IEEE Trans. Power Electron.,* vol. 20, no. 4, pp. 963–973, Jul. 2005.

[22] M. A. Elgendy, B. Zahawi and D. J. Atkinson, "Assessment of perturb and observe MPPT algorithm implementation techniques for PV pumping applications," *IEEE Trans. Sustain. Energy,* vol. 3, no. 1, pp. 21–33, Jan. 2012.

[23] D. C. Jones and R. W. Erickson, "Probabilistic Analysis of a Generalized Perturb and Observe Algorithm Featuring Robust Operation in the Presence of Power

Curve Traps," *IEEE Trans. Power. Electron.,* vol. 28, no. 6, pp. 2912–2926, Jun. 2013..

[24] M. A. S. Masoum, H. Dehbonei and E. F. Fuchs, "Theoretical and experimental analyses of photovoltaic systems with voltage and current-based maximum power-point tracking," *IEEE Trans. Energy Convers.,* vol. 17, no. 4, pp. 514–522, Dec. 2002 .

[25] A. Tariq and J. Asghar, "Development of an Analog Maximum Power Point Tracker for Photovoltaic Panel," in *IEEE PEDS*, 2005.

[26] T. Noguchi, S. Togashi and R. Nakamoto, "Short-Current Pulse-Based Maximum-Power-Point Tracking Method for Multiple Photovoltaic-and-Converter Module System," *IEEE Trans. Indus. Electron.,* vol. 49, no. 1, pp. 217–223, Feb. 2002.

[27] T. L. Kottas, Y. S. Boutalis and A. D. Karlis, "New Maximum Power Point Tracker for PV Arrays Using Fuzzy Controller in Close Cooperation With Fuzzy Cognitive Networks," *IEEE Trans. Ener. Conv.,* vol. 21, no. 3, pp. 793–803, Sep. 2006.

[28] L. S. Duan, F. Liu, B. Liu and Y. Kang, "A variable step size INC MPPT method for PV systems," *IEEE Trans. Ind. Electron.,* vol. 55, no. 7, pp. 2622–2628, Jul. 2008.

[29] M. A. G. D. Brito, L. Galotto, L. P. S. G. D. A. E. Melo and C. A. Canesin, "Evaluation of the Main MPPT Techniques for Photovoltaic Applications," *IEEE Trans. on Indus. Electron.,* vol. 60, no. 3, pp. 1156-1167, Mar. 2013.

[30] M. A. Elgendy, B. Zahawi and J. A. D, "Assessment of the Incremental Conductance Maximum Power Point Tracking Algorithm," *IEEE Trans. on Sust. Ener.,* vol. 4, no. 1, January 2013.

[31] "online," [Online]. Available: http://www.mathworks.com/matlabcentral/ fileexchange/34752-grid-connected-pv-array..

[32] G. M. S. Islam, A. A. Durra, S. Muyeen and J. Tamura, "Low Voltage Ride Through Capability Enhancement of Grid Connected Large Scale Photovoltaic System," in *IECON 2011 - 37th Annual Conference on IEEE Industrial Electronics Society*, Melbourne, 2011.

[33] [Online]. Available: http://www.vde.com/de/fnn/dokumente/documents/transmissioncode%202007_eng

l.pdf.

[34] [Online]. Available:
      http://www.bdew.de/internet.nsf/id/A2A0475F2FAE8F44C12578300047C92F/$fil
      e/BDEW_RL_EA-am-MS-Netz_engl.pdf.

[35] M. Taghizadeh, J. Sadeh and E. Kamya, "Protection of grid connected photovoltaic
      system during voltage sag," in *2011 International Conference on Advanced Power
      System Automation and Protection.*, Beijing, 2011.

[36] N. H. Viet and A. Yokoyama, "Impact of fault ride-through characteristics of high-
      penetration photovoltaic generation on transient stability," in *International
      Conference on Power System Technology Dec. 2010*, Dec. 2010.

[37] C. Photong, C. Klumpner and P. Wheeler, "A current source inverter with series
      connected AC capacitors for photovoltaic application with grid fault ride through
      capability," in *35th Annual Conference of IEEE on Industrial Electronics (IECON)*,
      Porto, Nov. 2009.

[38] M. Jafari, S. B. Naderi, M. T. Hagh, M. A. and S. H. Hosseini, "Voltage Sag
      Compensation of Point of Common Coupling (PCC) Using Fault Current Limiter,"
      IEEE Trans. on Power Delivery, vol. 26, no. 4, pp. 2638 - 2646, Oct 2011.

[39] M. H. Ali and R. Douga, "A closed-loop control based braking resistor for
      stabilization of wind generator system," in *IEEE Southeastcon,* , Charlotte, 2010.

[40] H. Hooshyar and M. E. Baran, "Fault Analysis on Distribution Feeders with High
      Penetration of PV Systems," *IEEE Trans. Power System,* vol. 28, no. 3, pp. 2890-
      2896, Aug. 2013.

[41] "IEEE Recommended Practice for Utility Interface of Photovoltaic (PV) Systems,"
      IEEE 929, 2000.

[42] E. Troester, "New German grid codes for connecting PV systems to the medium
      voltage power grid," in *in proc. 2nd International Workshop on Concentrating
      Photovoltaic Power Plants: Optical Design, Production, Grid Connection*,
      Darmstadt, Germany., Mar. 2000.

[43] W. A. Omran, M. Kazerani and M. M. A. Salama, "Investigation of methods for
      reduction of power fluctuations generated from large grid-connected photovoltaic
      systems," *IEEE Trans. Energy Conversion,* vol. 26, no. 1, pp. 318-327, 2011.

[44] K. Dragoon and A. Schumaker, "Solar variability and grid integration," Renewable Northwest Project (October, 2010). [Online].Available:http://www.rnp.org/sites/default/files/pdfs/Solar%20PV%20Variability%20and%20Grid%20Integration%20Oct%202010.pdf.," Renewable Northwest Project [Online].Available:http://www.rnp.org/sites/default/files/pdfs/Solar%20PV%20Variability%20and%20Grid%20Integration%20Oct%202010.pdf., October, 2010.

[45] A. Murata, H. Yamaguchi and K. Otani, "A method of estimating the output fluctuation of many photovoltaic power generation systems dispersed in a wide area," *Electrical Engineering in Japan,* vol. 166, no. 4, pp. 9–19, March 2009.

[46] A. Mills and R. Wiser, "Implications of Wide-Area Geographic Diversity for Short-Term Variability of Solar Power," Lawrence Berkeley National Labratory, September 2010.

[47] T. E. Hoff and R. Perez, "Quantifying PV power Output Variability," *Solar Energy,* vol. 84, pp. 1782–1793, 2010.

[48] E. Wiemken, H. Beyer and W. H. Kiefer, "Power characteristics of PV ensembles: experiences from the combined power production of 100 grid connected PV systems distributed over the area of Germany," *Solar Energy,* vol. 70, no. 6, 2001.

[49] S. M. Shaahid and M. A. Elhadidy, "Economic analysis of hybrid photovoltaic-diesel-battery power systems for residential loads in hot regions: A step to clean future," *Renewable Sustainable Energy Rev.,* vol. 12, no. 2, pp. 488-503, 2008.

[50] B. K. Bala and S. A. Siddique, "Optimal design of a PV-diesel hybrid system for electrification of an isolated island: Sandwip in Bangladesh using genetic algorithm," *Energy Sustainable Dev.,* vol. 13, no. 1, pp. 137-142, 2009.

[51] P. Arun, R. Banerjee and S. Bandyopadhyay, "Optimum sizing of photovoltaic battery systems incorporating uncertainty through design space approach," *Solar Energy,* vol. 83, no. 7, pp. 1013-1025, 2009.

[52] W. A. Omran, M. Kazerani and M. M. A. Salama, "Investigation of methods for reduction of power fluctuations generated from large grid-connected photovoltaic systems," *IEEE Trans. Energy Conversion,* vol. 26, no. 1, pp. 318-327, 2011.

[53] T. Gunen, Electric Power Distribution System Engineering, 2nd ed., Taylor & Francis Group, CRC Press, pp. 192 , 2008.

[54] M. H. Ali, W. Bin and R. Dougal, "An Overview of SMES Applications in Power and Energy Systems," *IEEE Transactions on Sustainable Energy ,* vol. 1, no. 1, pp. 38 - 47, April 2010 .

[55] S. Diaf, M. Belhamel, M. haddadi and A. Louche, "Technical and economic assessment of hybrid photovoltaic/wind system with battery storage in Corsica island," *Energy Policy,* vol. 36, no. 2, pp. 743-754, 2008.

[56] P. Thounthong, "Model based-energy control of a solar power plant with a supercapacitor for grid-independent applications," *IEEE Trans. Energy Conversion,* vol. 26, no. 4, pp. 1210-1218, 2011.

[57] D. C. Das, A. Roy and N. Sinha, "GA based frequency controller for solar thermal– diesel–wind hybrid energy generation/energy storage system," *Electrical Power and Energy Systems,* vol. 43 , pp. 262–279, 2012.

[58] N. Kakimoto, H. Satoh, S. Takayama and K. Nakamura, "Ramp-rate control of photovoltaic generator with electric double-layer capacitor," *IEEE Trans. Energy Conversion,* vol. 24, no. 2, pp. 465-473, June 2009.